MAR 27 1992

ORNL
MASTER COPY

ORNL/NPR-92/8

ornl

OAK RIDGE
NATIONAL
LABORATORY

MARTIN MARIETTA

INTERIM

PIPE BREAK TESTING OF PRIMARY LOOP PIPING SIMILAR TO DEPARTMENT OF ENERGY'S NEW PRODUCTION REACTOR—HEAVY WATER REACTOR

Materials/System Integrity Task of the HWR-NPR Program

Oak Ridge National Laboratory

[redacted]

[redacted]

Full public release
4/26/2013

MANAGED BY
MARTIN MARIETTA ENERGY SYSTEMS, INC.
FOR THE UNITED STATES
DEPARTMENT OF ENERGY

This report was prepared as an account of work sponsored by an agency of the United States Government. Neither the United States Government nor any agency thereof, nor any of their employees, makes any warranty, express or implied, or assumes any legal liability or responsibility for the accuracy, completeness, or usefulness of any information, apparatus, product, or process disclosed, or represents that its use would not infringe privately owned rights. Reference herein to any specific commercial product, process, or service by trade name, trademark, manufacturer, or otherwise, does not necessarily constitute or imply its endorsement, recommendation, or favoring by the United States Government or any agency thereof. The views and opinions of authors expressed herein do not necessarily state or reflect those of the United States Government or any agency thereof.

ORNL/NPR-92/8

New Production Reactor

INTERIM

PIPE BREAK TESTING OF PRIMARY LOOP PIPING SIMILAR TO DEPARTMENT OF ENERGY'S NEW PRODUCTION REACTOR—HEAVY WATER REACTOR

A. B. Poole
R. L. Battiste
J. A. Clinard
W. R. Hendrich

Materials/System Integrity Task of the HWR-NPR Program

Oak Ridge National Laboratory

January 1992

[redacted]

Prepared by the
OAK RIDGE NATIONAL LABORATORY
Oak Ridge, Tennessee 37831
managed by
MARTIN MARIETTA ENERGY SYSTEM, INC.
for the U.S. Department of Energy
under Contract No. DE-AC05-84OR21400

[redacted]

CONTENTS

	Page
LIST OF FIGURES	iv
LIST OF TABLES	vi
1. EXECUTIVE SUMMARY	1
2. INTRODUCTION	3
3. BACKGROUND	3
4. POSSIBLE PIPE RUPTURE SOURCES	4
5. DISCUSSION	6
6. FATIGUE DAMAGE ESTIMATION	7
7. FATIGUE CRACK GROWTH ANALYSIS	8
8. CRACK GROWTH	10
9. WORST CASE FLAW	10
10. PIPE LOADING CONDITIONS	10
11. TEST FACILITY DESIGN	11
12. DATA COLLECTION/INSTRUMENTATION	12
13. TESTING HISTORY AND RESULTS	13
14. MATERIAL TESTING AND FLAW DATA	19
15. CONCLUSIONS	20
16. ACKNOWLEDGMENTS	21
17. REFERENCES	21
APPENDIX A. Data Collection and Instrumentation Details	25
APPENDIX B. Fatigue Crack Growth Methods	29
APPENDIX C. Fracture Mechanics Analysis	31
APPENDIX D. Pipe Modal Analysis	33

LIST OF FIGURES

Figure		Page
1	Double-Ended Guillotine-Break	37
2	Failure of Circumferentially Cracked Pipe Under Seismic Loading	37
3	Comparison of Net-Section Collapse Criteria With Pure Bending Data on Stainless Steel Pipes with Through-Wall Flaws	38
4	NPR-HWR Plant	39
5	RCS-1 of 6 Loops Elevation View	40
6	Definition of Blocks and Subblocks for Fatigue Cycling	41
7	Crack Growth Rate Versus Stress Intensity	42
8	16-Inch Diameter Pipe/Schedule 40/Crack Growth for 60 Years	43
9	Worst Case Degraded Pipe 60 years	44
10	Pipe Impact Test Facility at ORNL	45
11	Pipe Impact Test Facility at ORNL	45
12	Pipe Impact Test Facility at ORNL	46
13	Pipe Test Specimen at ORNL	46
14	Data Collection Method	47
15	Load Versus Time	48
16	Deflection Versus Time	48
17	Weld Metal Strain Versus Time	49
18	Pressure Versus Time	49
19	Crack Opening Versus Time	50
20	Crack Growth Versus Time	50
21	Accelerometer A6 Versus Time	51
22	Accelerometer A7 Versus Time	51
23	Accelerometer A8 Versus Time	52
24	Accelerometer A9 Versus Time	52
25	Flow Rate Out of Crack Versus Length of Crack	53
26	Material Specimens From Pipe Coupons	54

LIST OF FIGURES (Con't)

Figure		Page
27	Crack Extension and Plastic Zone Deformation During Compliance Loading	55
28	Strain gage and Crack Propagation Gages Located on Pipe	56
29	Location of Accelerometers and DCDTs on Pipe	57
30	J Versus Crack Size for Test Pipe	58
31	Tmat Versus Crack Size for Test Pipe	59
32	Estimated J_{IC} for ORNL Compliance Tests	60

LIST OF TABLES

Table		Page
1	Estimated NPR-HWR Piping Transient Loading Cases	9
2	Estimated NPR-HWR Primary Pipe Loadings	11
3	ORNL Pipe Break Testing Overview	14
4	Piping Material Data	20
1.D	Dry Modal Test Results	35
2.D	Wet Modal Test Results	36

1. EXECUTIVE SUMMARY

Oak Ridge National Laboratory is conducting a task for the Department of Energy to demonstrate that the primary piping of the New Production Heavy Water Reactor (NPR-HWR), with its relatively moderate temperature and pressure, cannot suffer an instantaneous Double-Ended-Guillotine-Break (DEGB) under design basis loadings and conditions. Demonstration tests of flawed pipes under extreme loads that bound the bending moments induced by the Safe Shutdown Earthquake (SSE) are being conducted to provide data concerning the pipe failure mode and failure characteristics such as crack propagation rates, break opening times, and break size. Because highly ductile and crack resistant stainless steel material is employed for the large primary pipes and because the piping stresses for non-earthquake loadings are relatively small, the failure mode anticipated for the demonstration tests is one of dynamic-load-induced stable crack growth culminating in a net-section collapse of the pipe section containing a large circumferential flaw. Large margins to avoid the demonstrated pipe failures are expected and will be quantified in the subject pipe test program.

The intended end usage of the data and demonstration is to provide the NPR-HWR designer with a proven calculational method, based on conservative usage of elastic-plastic fracture mechanics theory, that when applied will quantify bounds on failure times (during occurrence of the plant's SSE earthquake) for various postulated cracks in the large primary piping. The instantaneous DEGB of the large piping will be replaced with a rational loss of coolant accident (LOCA). The substitution of the realistic LOCA will potentially lead to system design improvements and lower costs.

The test program began in March of 1991 with the design and construction of a facility, the Pipe Impact Test Facility (PITF), that is capable of applying static and impact loadings to the pipe test article that exceed by several times the bending moments estimated for the primary piping under SSE earthquake conditions. The PITF was completed in September 1991. Two test articles, 20 ft. long, 16 in. diameter, schedule-40 straight pipes of stainless steel 316L material, were fabricated to standards following the nuclear industry practices. The two pipes contain a circumferential weld at their centers. The pipe welds contain a

compound flaw/crack as an initial condition for impact testing. The initial flaw is sized to bound the estimated worst-case fatigue flaw that HWR piping could see in 60 years of service for the hypothetical situation where leak detection systems and crack inspection systems fail to notice the flaw's existence.

Each of the two test articles are to be tested to failure. The first pipe test began in October 1991 with a general test plan to explore the failure margin on crack size to reach unstable conditions for a dynamic load level of one times the SSE earthquake moment. The second pipe test will follow and will explore the failure margin on crack size for a load level of several (probably three-to-four) times the SSE earthquake moment.

Since October 1991, the first test article has been subjected to considerable overloadings. The pipe has been impacted over 40 times (four sequences of ten impacts) at levels equal to and beyond the SSE loading level. In addition over 300,000 fatigue cycles, and several purposeful static monotonic overloads have been applied in order to extend the flaw to help establish the data necessary to confirm fracture mechanics theories. The through-wall portion of the compound crack is, at this writing, more than seven times its original length. Crack growth during dynamic loadings remains stable with no apparent crack extension for most impacts and with modest extension for only four of the dynamic loadings. In all cases but one, crack extension occurred in only the first impact of the multiple impact test sequences.

This interim report is a sketch of the background information and of the test data and observations that have thus far been recorded. One intended purpose is to provide preliminary information to potential reviewers. Indeed, a critical portion of the data development process will be independent technical review by senior review groups. This element is considered crucial to the eventual acceptance of data and methods that come out of the ORNL pipe impact test program.

2. INTRODUCTION

The United States Department of Energy (DOE) is designing a new generation of production reactors intended to replace the aging production reactors at the Savannah River Site (SRS) in Aiken, South Carolina. A heavy water reactor is one of the options being pursued during the Title 1 design phase. The increases in understanding and the vast experience gained from existing production reactors and commercial nuclear power plants have led to proposed improvements in several areas of the design for the NPR-HWR.

One such area of improvement is to show that the tough austenitic piping of the NPR-HWR at moderate temperatures and pressures can provide a design that is not susceptible to a DEGB.

The PITF at ORNL has been designed to load pipes in bending. The maximum bending stress is located at the center of the pipe. The pipe is loaded in four point bending as shown on Fig. 29. This loading condition provides a constant bending stress across the 3 ft long center section of the pipe. The flaw being studied is at a weld in the exact center of the 3 ft constant bending section of piping. Both static and dynamic loadings can be used to produce bending in the pipe. This bending load tends to open the flaw as shown on Fig. 2. Therefore, the PITF can be used to show crack stability in tough austenitic piping.

3. BACKGROUND

The "maximum hypothetical accident" is a term used to describe what has generally become known as a DEGB. The concept was originated by the U.S. Atomic Energy Commission for the multiple purpose of sizing containments and establishing "accident" doses and later for sizing emergency core cooling systems. The original concept was quite straight forward; namely, an instantaneous DEGB of a major pipe (see Fig. 1) in the high-energy primary system of a light-water reactor would maximize the fluid release and establish an upperbound for the design pressure established for a containment. This determined the containment volume in relationship to a reasonable design accident pressure.

Later changes in regulatory philosophy, primarily with regard to seismic design, tended to shift the DEGB from a hypothetical accident to one with increasing credibility. At present the regulatory practice requires inclusion of the large pipe instantaneous DEGB for modeling and sizing the emergency core cooling system (ECCS) of commercial power reactors.

The application of fracture mechanics technology in the licensing process [1] to demonstrate the integrity of nuclear facility high-energy piping systems, in lieu of requiring the postulation of a nonmechanistic DEGB, has become known as leak-before-break (LBB). The LBB approach originated some years ago to resolve the asymmetric load issue for certain pressurized water reactor (PWR) facilities. The LBB rationale has been extended to allow the removal of large and massive pipe restraints in numerous PWR facilities. Discussions of the fracture mechanics technology and results of both analysis and tests are extensive in the literature [2-9].

The primary coolant pressure and temperature of an NPR-HWR are significantly less than in PWR facilities. The NPR-HWR design represents a moderate-energy system rather than a high-energy system. The moderate-energy of the primary coolant allows the use in the NPR-HWR of smaller diameter, thinner walled, and highly ductile stainless steel piping. In addition, the design of this stainless steel piping will take full advantage of improved materials which have been shown to be highly resistant to stress corrosion cracking. The piping design loads for the NPR-HWR are significantly smaller in all areas than those of PWR facilities, with the possible exception of seismically induced bending moments. Therefore, the major design loadings relative to potential NPR-HWR pipe breaks are the seismic loads.

4. POSSIBLE PIPE RUPTURE SOURCES

The three most possible sources that could contribute to a DEGB are: (1) heavy loads falling from a crane onto the pipe, (2) failure of axial flaws due to subcritical crack growth followed by an overpressurization event, and (3) circumferential flaws growing from corrosion/fatigue crack growth and subsequent seismic loading.

Heavy Loads. The movement of major heavy loads inside the containment building during operation is very rare and generally minimized by operating instructions. The design of the

plant layout and use of operating instructions make such a piping failure mechanism too improbable to be realistic.

Failure of an Axially Cracked Pipe. For a low-pressure, stainless steel, piping system like NPR-HWR it is considered impossible to cause a pipe overpressurization that would be large enough to provide a rupture equivalent to a DEGB due to an axial crack. Fracture mechanics would show that only a small break could occur.

Failure of a Circumferentially Cracked Pipe Under Seismic Loading. The most probable cause of a DEGB pipe break is the possibility of a circumferential flaw growing by corrosion/fatigue crack growth over time and resulting in failing by a seismic overload. The maximum seismic moment loads for the NPR-HWR piping system are low enough that they could not cause pipe failure except for a case where a through wall flaw exists essentially half-way around the pipe. Achieving a flaw of this magnitude is considered highly improbable to achieve in the Type 316LN stainless steel piping. The worst case base metal and weld metal corrosion/fatigue flaws are discussed and estimated in this report. It is these worst case flaws that were tested at maximum seismic loads and beyond to ensure that they are stable and can not lead to a DEGB. The failure mechanism of the ductile stainless steel piping is shown in Fig. 2. The crack stability of a 16 in. diameter, Schedule 40, Type 304 stainless steel pipe has been significantly benchmarked [10] for a pressurized condition (1378 psi) at 550° F by numerous investigators.

Typically, in a DEGB evaluation of dynamic effects from a pipe break, the pipe rupture is assumed to be instantaneous. This assumption was based on extremely conservative linear elastic fracture mechanics considerations made several decades ago. Since then, fracture speeds have been found to be much slower than originally assumed for a circumferential crack in a ductile material such as Type 316LN stainless steel. The tests discussed in this report have established crack opening and crack closing times for the worst case seismic loadings at NPR-HWR pressure and temperature. During these tests actual crack propagation times have been established. It is shown that even for these large overload conditions actual pipe parting did not occur. The safety of the NPR-HWR primary piping is shown on Fig. 3. Figure 3 provides actual pipe load tests and their failure stress correlated with

net-section-stress failure criterion. The worst case NPR-HWR 60-year flaws are well within the safe area of the criterion and provide large margins on loading and corrosion/fatigue crack growth.

5. DISCUSSION

A conceptual design for the HWR-NPR is shown in Fig. 4. The reactor vessel height would be 8.37 m (329.5 in.) with an outside diameter of 6.25 m (246.0 in.) and a wall thickness of 0.076 m (3 in.). The normal operating pressure is estimated to be approximately 1.034 MPa (150 psi) and the reactor outlet temperature approximately 110°C (230°F). The use of Type 316LN or 316NG stainless steel as the pressure vessel material and primary piping material will be adopted to provide the best available material that features the necessary strength, pressure-retaining and corrosion-resistant characteristics [11-13].

In the NPR-HWR plant design the Primary Water System (PWS) is required to circulate heavy water (D_2O) through the reactor to remove heat produced in the reactor from the fission process, the absorption of gamma radiation, and the decay of fission products. Cooling is provided for fuel assemblies, target assemblies, control rods, bulk moderator, core internals, shielding, and the reactor vessel. In addition to serving as the heat transfer medium, the process fluid moderates neutrons produced by fission in the fuel. D_2O is used in this application because of its favorable moderating and neutron capture properties, which results in high neutron efficiency and reactor productivity. The PWS components must also provide a high-integrity leak barrier against a loss of moderator and the radioactive fission and corrosion products.

The PWS will consist of several parallel heat transfer loops. Each of the heat transfer loops will have one or more pumps and heat exchangers. One or more loops are expected to be connected with a pressurizer and/or accumulator which may have an overpressure of nitrogen or other inert gas. The pumps deliver water through the loop from reactor vessel to heat exchanger(s) and back to the reactor vessel. The piping from reactor vessel to heat exchanger has an outside diameter of 0.405 m (16 in.) and a wall thickness of 0.013 m (.5 in.). The heat exchangers use light water (H_2O) to control the D_2O temperature during operation.

The maximum heavy water temperature should be <110°C (230°F) at the reactor outlet. An early design concept of the main loop piping is shown on Fig. 5 with piping run length of approximately 6 m (20 ft).

6. FATIGUE DAMAGE ESTIMATION

Estimating fatigue damage in the stainless steel reactor primary piping is difficult because the complete characterization of the thermal loads have not been available, and the technology to accurately predict defect propagation in the welds is not fully developed.

The imperfections, residual stresses, and geometry of the welds in the piping circumferential direction make them the most suspect location for fatigue damage. The microstructure of the weld metal, related yield and tensile strengths, residual stresses, loading conditions, and surface conditions strongly effect defect propagation associated with weld imperfections [14]. The material properties near imperfections may be locally degraded, and this degradation must be taken into account to evaluate the effect of the microstructure on defect propagation. The welding residual stresses increase the mean stress and, therefore, play a significant role in low-stress, high-cycle fatigue because the shake-down effect is absent, and the fatigue life may be reduced by a factor of two to three [15-17]. A fatigue crack growth analysis needs to be part of the design process for the NPR-HWR primary pressure piping. This analysis is needed to determine if special welding processes are required to reduce weld residual stress levels in order to preclude crack growth through the piping wall over 60-years of operation. A conservative approach to this analysis is to assume an existing flaw at the piping inside wall surface.

7. FATIGUE CRACK GROWTH ANALYSIS

Fatigue crack propagation behavior can generally be described by a power law. For this analysis, the following generalization was used in the form:

$$da/dn = C(\Delta K_{eff})^n \text{ (in./cycle)} \quad (1)$$

See Appendix B for more details on the methodology.

In order to complete the crack growth analysis, several items had to be developed. These items are as follows:

1) Plant transient conditions (estimated)
2) Local primary piping loads (estimate)
3) Primary piping stress profile for transient conditions

PWR transients [18] were studied and modified to establish the estimated transients for NPR-HWR. These are listed in Table 1. In this review, some 32 transients were identified and then refined to a set of 23 transients that produce tension stress at the primary piping inner wall. By reviewing these 23 transients, it was possible to combine them into 10 subblocks as shown in Table 1. Each subblock has an equivalent load case Combined Transient Number (CBT) that provides a stress profile in the piping wall. These subblocks were used in a fatigue crack growth analysis as shown in Fig. 6. For this analysis, each block represented ten years of operation. The transient thermal stress was calculated for each transient [19] and added to the other stresses to provide the total axial stress state for the Type 316LN stainless steel primary piping. The fatigue crack growth for the primary piping weld was also studied. For analysis purposes, the estimate of weld residual stress was established and added to the other stresses. The weld residual stress was estimated based upon measured weld residual stresses from large pipes [20]. The fatigue crack growth studies were completed using the Upper-Bound Crack Growth Rate curve [21] that is shown on Fig. 7. Appendix B provides a more detailed discussion of fatigue crack growth analysis.

Table 1. Estimated NPR-HWR Piping Transient Loading Cases

Subblock No.	Stress Summary Load Case	Total Cycles for 60 Years	Equiv. Load Case at Cycles/Year
1	CBT3 Unit Unloading CBT5 Off-Normal Step Temp. Decrease CBT6&7 SS Avg. Fluct. CBT18 Normal Reactor Trip CBT1 Full Gas Purge	19,800 3,000 2,144,100 540 2,100	CBT5 at 36,159 Cycles/Year
2	CBT15 Normal Loop Startup CBT8&9 SS & Random Fluct. (7%) CBT10&11 SS & Random Fluct. (10%)	300 1,549,800 1,080,975	CBT10 at 43,851 Cycles/Year
3	CBT16 Normal Loop Shutdown CBT14 Cooling Water Cycling	300 3,000	CBT14 at 55 Cycles/Year
4	CBT12&13 SS & Random Fluct. (15%) CBT21 Inadvertent PWS Depressurization CBT17 Loss of Power	476,400 180 180	CBT12 at 7,946 Cycles/Year
5	CBT20 Reactor Trip with Accum. Inj. Cooldown	12	CBT20E at 1 Cycle/Year
6	CBT22 Fast Valve Closure $\Delta P = 6.5P$	600	CBT22 at 10 Cycles/Year
7	CBT19 Reactor Trip with Cooldown	240	CBT19 at 4 Cycles/Year
8	CBT26 Fast Valve Closure $\Delta P = 4.75P$	600	CBT26 at 10 Cycles/Year
9	CBT27 Fast Valve Closure $\Delta P = 2.9P$	600	CBT27 at 10 Cycles/Year
10	CBT32 Earthquake (OBE)	120	CBT32 at 2 Cycles/Year

8. CRACK GROWTH

The growth of possible small pre-existing defects in the piping wall was estimated over a plant life of 60 years using the computer program pc-CRACK [29]. This crack growth is for a semi-circular surface flaw at the inside pipe wall and located at the center of a circumferential weld. Primary piping total axial tension stresses tend to open this flaw and cause it to grow. The analysis was completed using two percentages of weld residual stress profile. These percentages were 100% and 0%. These results are presented in Fig. 8.

9. WORST CASE FLAW

Using the crack growth shown in Fig. 8, the worst case 60 year flaws were established as shown in Fig. 9. For the welded pipe, a 0.17 in. deep 360° circumferential crack at the pipe inside diameter was determined by crack growth over 60 years. The worst case flaw was determined to be a compound condition where a 1 in. long thru-wall flaw intersects the 360° circumferential flaw. Fracture mechanics analysis, has shown these worst case 60 year flaws to be well within the stability range of the NPR-HWR primary piping even when minimum material tearing properties are used in the analysis. Tearing instability is not predicted until a crack length 0.28 (πD) is obtained. This point of tearing instability is a thru-wall crack which is 14 times longer than the worst case 60 year flaw (i.e., 14 in. long). The dynamic testing program was designed to prove the existence of these large margin values.

10. PIPE LOADING CONDITIONS

An analysis of the NPR-HWR primary piping was completed using the current design basis. This loading condition is assumed to be present at a circumferential weld in the primary piping cold leg. In order to represent the seismic bending load in the pipe, a combined bending moment was established using the square root of the sum of the squares (SRSS) method. This moment is provided in the test pipe by four point bending. The actual test pipe is pressurized to 250 psi, which is a conservative over test condition. The water

temperature during impact testing was approximately 135°F and represents the NPR-HWR cold leg temperature. The pipe loading is shown in Table 2.

Table 2. Estimated NPR-HWR Primary Pipe Loading

LOAD TYPE	Axial Force (kips)	Bending Moments (ft-kips)	
	F(z)	M(x)	M(y)
Deadweight	3.99	4.85	0
Thermal	-1.10	-15.70	-15.70
SSE	±8.31	±62.10	±62.10
Seis. Anchor Motion	±0.21	±2.37	±2.37
Pressure	17.61	0	0
		-75.32	-80.17

$$\textit{Maximum Bending} = \sqrt{(75.32)^2 + (80.17)^2}$$

$$= 110 \text{ ft-kips}$$

The value of 110 ft-kips was established to represent the safe shutdown earthquake (SSE) pipe bending moment. Based upon the geometry of the PITF, this 110 ft-kip bending moment is applied to the test pipe when the load cell reads a value of 27.5 kips. Therefore, a load cell value of 27.5 kips is considered 1 SSE loading. This bending moment is also measured by strain gage XE-100 on the back side of the pipe. A compression strain of 0.0455% at gage XE-100 represents 1 SSE (22.5 kips) loading.

11. TEST FACILITY DESIGN

The piping impact test facility is shown in Figs. 10-13. The test piece is a 16-inch diameter schedule 40 stainless steel pipe. This pipe is approximately 20 ft long and has a circumferential weld at the center. The center weld was completed using a weld joint design that provided a lack of penetration 360 degrees around the pipe and 0.17 in. deep at the inside surface. This represents a worst case 60-year flaw at the pipe inside diameter. At the

center of the pipe weld, a 0.03 in. wide by 1 in. long slot was machined by metal disintegration from the outside pipe surface totally through the 0.5 inch thick pipe wall. This provided a worst case compound flaw as shown on Fig. 9.

The test facility design is such that the pipe can be loaded in bending using a 110 kip hydraulic ram and/or a 3100 lb swing weight. After the initial thru-wall flaw was machined into the pipe, it was covered over at the pipe surface by a 0.06 deep weld along the slot. The pipe was then fatigued in bending until a crack was developed completely along the cover weld. This crack was then extended into the circumferential weld by fatigue using the 110 kip hydraulic ram. At various crack lengths the flaw was tested by a dynamic impact loading using the 3100 lb swing weight. This dynamic load method has provided loads up to twice the seismic bending load calculated for the NPR-HWR plant (2 times SSE).

As of December 6, 1991, dynamic testing had been completed for crack lengths of 1.4, 1.7, 3.0, 4.2, and 4.6 in length. Small amounts of crack growth have been measured. But, the pipe remains intact and capable of more loading cycles. These loading cycles will be continued until net-section yielding of the pipe is obtained.

12. DATA COLLECTION INSTRUMENTATION

A high speed data system collects data during the 0.1 second dynamic event. The significant features of this system are as follows:

- 32,000 Synchronous scans/sec
- 24 Channels, nominally as below:
  - 1 Load cell
  - 1 Pressure cell
  - 2 Crack extension gages
  - 1 Crack opening gage
  - 5 Displacement measuring devices
  - 7 Accelerometers
  - 7 Strain gages

— Pretriggers for exact t = 0

— Sophisticated display software

— Data management software with built-in QA features

— Backup each night to tape

— Some analytical features, e.g. integration & differentiation

Descriptions and details of the data collection system and instrumentation types and locations are provided in Appendix A.

13. TESTING HISTORY AND RESULTS

Since October 1991, the test article has been subjected to considerable overloadings. The pipe has been impacted 40 times at levels equal to and beyond the SSE loadings. In addition, over 300,000 fatigue cycles and 4 purposeful static overloads have been applied in order to extend the flaw and to establish the data necessary to confirm fracture mechanics theories. Table 3 provides a summary of all testing completed to date. The pipe will continue to be overloaded until net-section collapse. It is estimated that at least two more series of tests must be accomplished before testing of this first pipe is completed.

13.1 TEST RESULTS

For a general description, test number 6 (Hit-0) will be described. This testing was completed on November 25, 1991. The basic test parameters are as follows:

Crack size — 4 in.

Drop height — 11-1/4 in.

Pressure — 250 psig

Temperature — 135°F

The test results are provided on Figs. 14-25. A summary of the results are provided as follows:

Peak impact loading — 100,000 lb

Peak bending load — 42,000 lb (1.5 SSE)

Maximum bending deflection — 0.54 in. (0.03 seconds after impact)

Table 3. ORNL Pipe Break Testing Overview

Thru-wall

Initial crack = 1000 mils

Date	Event	Temp °F	Press. psig	Result Crk. Total-Mils	Drop Ht in.	Max. Bend. load kips
21-Oct-91	Fatigue	Rm. temp.	0	1350	—	40
23-Oct-91	Overload	Rm. temp.	0	1360	—	70
23-Oct-91	Hit 4-0	130	250	1360	5.00	25
5-Nov-91	Fatigue	Rm. temp.	0	1680	—	30
5-Nov-91	Compliance	Rm. temp.	0	1680	—	30
6-Nov-91	P-flow check	130	250	1680*	—	0
7-Nov-91	Hit 4-1	130	0	1680	5.00	25
8-Nov-91	Hit 4-2	130	0	1680	5.00	25
11-Nov-91	Hit 4-3	130	0	1680	5.00	25
11-Nov-91	Hit 4-4	130	0	1680	5.00	25
13-Nov-91	Hit 4-5	130	0	1680	5.00	25
14-Nov-91	Hit 4-6	130	165	1680	5.00	25
14-Nov-91	Hit 4-7	130	180	1680	5.00	25
14-Nov-91	Hit 4-8	130	225	1680	5.00	25
14-Nov-91	Hit 4-9	130	230	1680	5.00	25
18-Nov-91	Compliance	Rm. temp.	0	1680	—	30
18-Nov-91	Compliance	Rm. temp.	0	1710	—	40
18-Nov-91	Compliance	Rm. temp.	0	1760	—	50

*This measurement is considered to be more accurate than those previous.

**Total of 10 hits in this series.

Date	Event	Temp °F	Press. psig	Result Crk. Total-Mils	Drop Ht in.	Max. Bend. load kips
18-Nov-91	Compliance	Rm. temp.	0	2400		60
18-Nov-91	P-flow check	108	250	2400*	—	0
19-Nov-91	Compliance	Rm. temp.	0	2400		30
19-Nov-91	Compliance	Rm. temp.	0	2400		40
19-Nov-91	Compliance	Rm. temp.	0	2400		50
20-Nov-91	P-flow check	130	250	2400	—	0
21-Nov-91	Fatigue	Rm. temp.	0	2930	—	40
**21-Nov-91	Hit 5-0	130	250	2950	5.00	25
21-Nov-91	thru 5-9	130	250	2950	5.00	25
21-Nov-91	Compliance	Rm. temp.	0	3000*	—	40
24-Nov-91	Fatigue	Rm. temp.	0	3320	—	30
25-Nov-91	Compliance	Rm. temp.	0	3320	—	30
**25-Nov-91	Hit 6-0	140	250	4000	11.25	42
25-Nov-91	thru 6-9	140	250	4000*	11.25	42
5-Dec-91	Fatigue	Rm. temp.	0	4100	—	20
5-Dec-91	Compliance	Rm. temp.	0	4100	—	20
5-Dec-91	Compliance	Rm. temp.	0	4100	—	33
5-Dec-91	Compliance	Rm. temp.	0	4100	—	41
6-Dec-91	Fatigue	Rm. temp.	0	4140	—	20
**6-Dec-91	Hit 7-0	140	250	4180	11.25	42
6-Dec-91	Hit 7-1	140	250	4180	11.25	42
6-Dec-91	Hit 7-2	140	250	4180	11.25	42
6-Dec-91	Hit 7-3	140	250	4600	15.25	52

Date	Event	Temp °F	Press. psig	Result Crk. Total-Mils	Drop Ht in.	Max. Bend. load kips
6-Dec-91	Hit 7-4	140	250	4600	15.25	52
6-Dec-91	thru 7-9	140	250	4600*	15.25	52
13-Dec-91	Fatigue	Rm. Temp.	0	7300	—	25
18-Dec-91	Compliance	140	250	7300	—	21
18-Dec-91	Compliance	140	250	7380	—	31
18-Dec-91	Compliance	140	250	7380	—	32
20-Dec-91	Compliance	145	250	7380	—	20
20-Dec-91	Compliance	145	250	7380	—	30
20-Dec-91	Compliance	145	250	7440	—	40
20-Dec-91	Compliance	145	250	7440	—	40
20-Dec-91	Compliance	145	250	7600	—	50
12-Jan-92	Visual	Rm. temp.	0	7600*	—	0

Maximum crack opening distance — 0.028 in. (max. bending)

Crack growth at top gage — 0.48 in. (half crack extension)

Maximum weld stress — 34,160 psi (axial, due to bending)

Equivalent pipe acceleration — ≈ 8 g's (accelerometers, A7-A8)

Maximum pipe wall acceleration — 106 g's (near crack)

Maximum swing hammer acceleration — 138 g's (at impact)

Crack motion occurred during the first impact load or hit 6-0. During the nine succeeding drops, the crack did not extend; however, crack blunting did cause leakage to increase.

The general method of data collection is shown on Fig. 14. In this figure, four various parameters measured during each impact are shown as a function of time. The significant impact loading occurs over approximately 0.15 seconds. The time between the first impact and the second impact (due to rebound) is approximately 1.7 seconds. The second impact

is inconsequential to the test observations and will not be further disucssed. The approximate relationships between pipe impact load and maximum pipe bending load are given by the following:

$$F_{Impact} = C_{Impact} \sqrt{k_1 h}$$

$$F_{Bending} = C_{Bending} \sqrt{k_1 h}$$

where:— C_{Impact} and $C_{Bending}$ are two different constants.

— k_1 is the stiffness constant for the pipe and changes as the crack grows (lb/in.).

— h is the height that the weight center of mass has been raised (in.).

After the first impact, the weight is in contact with the loading mechanism for 0.052 seconds. The impact data shown on Fig. 14 are for a small height release and are useful only relative to understanding the instrumentation and impact mechanism.

The load cell versus time data for test-6, hit-0 are shown on Fig. 15. The maximum impact load was 100,000 pounds and occurred at t = 0.090 seconds. The impact time zero is t = 0.087 seconds, approximately. The maximum bending load was 42,000 pounds (1.5 SSE) and occurred at t = 0.120 seconds. Other peak loads shown on Fig. 15 are seen by the load cell. The load at t = 0.145 seconds is the load caused by impact of the sliding ram with a dynamic stop on first backswing.

Figure 16 shows the center deflection of the pipe as measured by a DCDT. The maximum center deflection is 0.54 in. The first and second bending motions have peak deflections at t = 0.117 seconds and t = 0.163 seconds respectively. The second peak occurs after impact with the dynamic stop as mentioned above. The natural free vibration frequency of this pipe is seen in the second peak (after swing weight has lifted off) and is approximately 12 Hz.

Figure 17 shows the strain versus time data for strain gage XE-112. This strain gage was located on the pipe circumferential weld at a distance of 3 in. from the centerline (see Fig. 28). The strain gage was oriented along the pipe so that it measured the outer fiber bending

strain. The maximum strain measured was 0.122% and represents an approximate tension stress of 34,160 psi in the weld metal. The strain gage was located approximately 1 in. away from the top tip of the 4 in. long crack.

The fluid pressure in the pipe is shown as a function of time in Fig. 18. The maximum increase in pressure during the test was 81 psi and occurred at approximately t = 0.103 seconds. This pressure load, together with the pipe front wall motion, is why the peak strain gage measurement does not quite coincide with the peak bending motion as shown on Fig. 16. A review of strain gage XE-100, which is located 180 degrees from the flaw, shows that for all impacts the maximum strain was obtained at about time t = 0.105 seconds.

The maximum crack opening displacement (COD) was 0.028 inches and occurred at t = 0.12 seconds, as shown on Fig. 19. This maximum COD is near the point of maximum pipe bending motion as would be expected. The COD data and the pressure transducer data show a frequency content of approximately 500 Hz. This value is close to the calculated breathing mode frequency of the impacted 3 foot long section of piping (see Appendix D).

The top crack growth gage data are shown on Fig. 20. Prior to the dynamic test, the crack length had been grown by bending fatigue of the pipe until the crack was visually determined to be essentially at the first wire of the crack gage. During the hit 6-0 impact, this top crack gage showed a crack extension totally through the gage (all 20 wires). Visual examination after the test determined the crack to have extended approximately 0.08 inches beyond the last wire on the gage. It should be noted that this visual measurement was made through the wire break gage. The plastic zone in the metal may have influenced this observation. However, for conservatism, the 0.08 in. is included as crack growth and this provided for a crack extension of 0.48 inches during the impact. Figure 20 shows that the last wire (No. 20) was broken at the same time that strain gage XE-112 recorded the maximum strain t = 0.107 seconds. The time required to break all the gage wires was 0.004 seconds. This provides a bound on crack extension speed of 120 inches per second.

Figures 21-24 show the various accelerometer data taken during hit 6-0. These acceleration data are provided in in./s^2 versus time. Accelerometer A6 is located on the front wall (crack side of the pipe) 5 in. east of the pipe centerline (see Fig. 29). Accelerometer

A7 is located on the back wall of the pipe two in. east of the pipe centerline. Accelerometer A8 is located on the rigid pipe load frame six in. east of the pipe centerline and does not see pipe wall flexibility effects, and therefore, can be compared with A6 and A7 to establish the pipe wall motion. Accelerometer A9 is mounted on the rear (impact end) of the hydraulic ram support. The A9 accelerometer picks up the direct hammer impact and also the ram rebound when the hammer completes a reverse swing and lifts off of the load train.

Figure 25 shows the leakage flow rates out of the pipe flaw for various size cracks. The test pipe is pressurized by nitrogen overpressure to a stand-pipe filled with water. The flow meter is located in a small diameter pipe that is between the stand-pipe and the test pipe. All flow that leaves the test pipe through the crack is measured by the flow meter. The flow meter lags the dynamic event somewhat, but provides a good measure of pipe leakage. These leakage values have also been obtained during static pipe loadings for different size cracks.

14. MATERIAL TESTING AND FLAW DATA

During fabrication of the stainless steel 316L test pipes, several test coupons were prepared using the production materials and weld metal heats. These coupons were made by the same welders and process that was used to fabricate the test pipes. In order to evaluate test data, several material tests are to be conducted from the coupon material. Table 4 provides the certification properties of the pipe heats and Fig. 26 shows the locations and types of material test coupons that will be evaluated. This testing is currently in progress. The test pipe material was ordered as type 316L; however, the actual chemistry shows it to be essentially 316LN material.

Table 4. Piping Material Data

Material -Type 316L Stainless Steel
ASTM-312 (welded pipe)
16-in. O.D. by 0.500 in. wall

Chemical Composition

Heat	C	Mn	P	S	Si	Ni	Cr	Mo	Co	Cu	N
27026	.011	1.65	.029	.020	.42	10.16	16.47	2.10	.12	.24	.075
27024	.020	1.76	.033	.019	.43	10.20	16.43	2.10	.12	.23	.071

Mechanical Tests

Heat	Tensile Strength, psi	Yield, psi	% Elong.	R of A %	Hardness	psi Hydro
27026	83,500 Transverse Test 87,090	40,000 49,630	56.4 54	61.4	B78-81	800
27024	84,500 Transverse Test 85,950	42,800 52,060	56.4 55	63.5	B77-79	800

Weld Wire

Spec.	Size	Alloy	Heat No.
AWS A5.9-B.1/	1/16" x 36	316L	IF26A05141D
ASME SFA5.9/	3/32" x 36	316L	IF28E05311AA
ER316L	1/8" x 50#	316L	IF26A07270G1

15. CONCLUSIONS

Testing to date confirms that crack growth under dynamic SSE load levels is stable and demonstrates that the instantaneous DEGB is not probable for the moderate energy system of the NPR-HWR when loaded at a 1 SSE loading condition. Hits 4-0 through 4-9 as shown

in Table 3 provides proof of crack stability for a worst case flaw at the 1 SSE level. Also, as of December 6, 1991 the pipe with through wall flaw lengths ranging from 1.4 inches to 4.6 inches was impacted at total of 40 times at 1 SSE and beyond with no unstable crack growth.

For hit 6-0 a crack growth of 0.48 inches occurred in 0.004 seconds based upon the top crack growth gage. This provides a half flaw growth rate of 120 in/sec. This value is very close to that measured by other investigators for stable crack growth in steel [30]. When the crack is growing in the unstable region, growth rates could be on the order of 8,000 in/sec as reported for unstable ductile fracture rates in steel pipe lines [31]. Thus, it is shown that all crack growth in this test has been in the stable region.

For a NPR-HWR primary pipe with the worst case 60-year flaw, it is estimated that as a minimum 14 full bending cycles of at least 1.5 SSE magnitude would be required to totally part the pipe. This assumes no crack blunting which has not been the case in these tests. For the 40 impacts, a crack growth occurred only during the 1st or 2nd of a series and only crack blunting was seen during the remaining impacts in a series. Under these most conservative of assumptions, it would take 1,400 milliseconds, as a minimum, to part the pipe. The effect of crack blunting would significantly increase this time and require loads equal to or beyond 2 SSE levels to tear the pipe. These conclusions are based upon testing completed to date. Additional data will be available at a later date to establish crack instability sizes and crack propagation times.

16. ACKNOWLEDGMENTS

The authors wish to acknowledge the help and interest provided by Mr. J. J. Jicha, Jr. of the Office of New Production Reactors Program, Department of Energy.

17. REFERENCES

1. *Report of the U.S. Nuclear Regulatory Commission Piping Review Committee,* prepared by The Pipe Break Task Group, NUREG-1061, Vol. 3, November 1984.

2. 1983 ASME Boiler and Pressure Vessel Code, Section XI - Rules for In-Service Inspection of Nuclear Power Plant Components, Article IWB-3640, Evaluation Procedures and Acceptance Criteria for Austenitic Piping.
3. Kanninen, M. F., et al., *Mechanical Fracture Predictions for Sensitized Stainless Steel Piping with Circumferential Cracks,* Final Report, EPRI NP-192, September 1976.
4. Winter 1985 Addendum, ASME Boiler and Pressure Vessel Code, Section XI - Rules for In-Service Inspection of Nuclear Power Plant Components, Article IWB-3640, Evaluation Procedures and Acceptance Criteria for Austenitic Piping.
5. Kanninen, M. F., et al., *Instability Predictions for Circumferentially Cracked Type 304 Stainless Steel Pipes Under Dynamic Loading,* Final Report on EPRI Project T118-2 by Battelle Columbus Laboratories, EPRI Report Number NP-2347, April 1982.
6. Paris, P. C. and Tada, H., *The Application of Fracture Proof Design Methods Using Tearing Instability Theory to Nuclear Piping Postulating Circumferential Through Wall Cracks,* NUREG/CR-3464, September 1983.
7. Klecker, R., Brust, F. W., and Wilkowski, G., *NRC Leak-Before-Break (LBB.NRC) Analysis Method for Circumferentially Through-Wall-Cracked Pipes Under Axial Plus Bending Loads,* Battelle Columbus Division, Topical Report to NRC, Contract No. NRC-04-84-103, NUREG/CR-4572, BMI-2134, March 1986.
8. Kumar, V., German, M. D., and Shih, C. F., *An Engineering Approach for Elastic-Plastic Fracture Analysis,* EPRI Final Report NP-01931, July 1981.
9. Kumar, V., et al., *Advances in Elastic-Plastic Fracture Analysis,* EPRI Final Report NP-3607, August 1984.
10. Kanninen, M. F., et al., *CSNI/NRC Workshop on Ductile Piping Fracture Mechanics,* NUREG/CP-0075, Proceedings of workshop held in San Antonio Texas, June 21-22, 1984.
11. NPR Programs Staff, *Materials Evaluation for the NPR-HWR,* ORNL/NPR-90/1.
12. NPR Programs Staff, *NPR-HWR Materials/System Integrity Corrosion Test Plan,* ORNL/NPR-90/2.

13. NPR Programs Staff, *NPR-HWR Materials/System Integrity Mechanical Behavior and Irradiation Effects Test Plans,* ORNL/NPR-90/3.

14. Lundin, C. D., "Bibliography on Fatigue of Weldments and Literature Review on Fatigue Crack Initiation from Weld Discontinuities," Welding Research Council Bulletin 333, May 1988.

15. Shah, V. N. and Conley, D. A., "Research Needs for Fatigue Damage Assessment in PWR Surge and Spray Piping," Transactions of SMiRT 10 International Conference, Vol. F, August 1989, pp. 87-92.

16. Boyles, L. G., "Case Histories of Failures Involving Residual Stresses," Fatigue, Fracture, and Risk, PVP-Vol. 215, June 1991, pp. 101-110.

17. Angelsen, S. O. and Saugerud, O. T., "A Probabilistic Approach to Ammonia Pressure Vessel Integrity Analysis," Fatigue, Fracture, and Risk, PVP-Vol. 215, June 1991, pp. 59-65.

18. Svensson, P. O., *Assessment of LWR Piping Design Loading Based on Plant Operating Experience,* Report No. 01-0880-1083 Rev. 0 prepared by EDS Nuclear Inc. for U.S. Department of Energy under Sandia National Laboratories Contract No. 13-7180, 1980, pp. D-3 through D-21.

19. Zudans, Z., Yen, T. C. and Steigelmann, W. H., Thermal Stress Techniques in the Nuclear Industry, American Elsevier Publishing Co., Inc., New York, 1965, pp. 94-111.

20. Hazelton, W.S. and Koo, W. H., *Technical Report on Material Selection and Processing Guidelines for BWR Coolant Pressure Boundary Piping,* NUREG-0313 Rev. 2, 1988, page A.8.

21. Yahr, G. T., Richardson, A. K., Gwaltney, R. C., and Sever W. L., *Case Study of the Propagation of a Small Flaw under PWR Loading Conditions and Comparison with the ASME Code Design Life,* NUREG/CR-3982, ORNL-6099, for U.S. Department of Energy, 1984, page 24.

22. Database for Environmental Crack Model Development, maintained for EPRI by Battelle-Columbus Laboratories.

23. James, L. A., "Fatigue-Crack Growth Correlations for Design and Analysis of Stainless Steel Components," Pressure Vessel and Piping Division of the ASME, 82-PVP-25.
24. James, L. A., "Fatigue-Crack Propagation in Austenitic Stainless Steels," *At. Energy Rev. 14(1)*, 37-86, 1976.
25. James, L. A., "The Effect of Elevated Temperature Upon the Fatigue-Crack Propagation Behavior of Two Austenitic Stainless Steels," *International Conference on Mechanical Behavior of Materials, 1st Kyoto, 1971 Proceedings*, 3, 1972, pp. 341-52.
26. Shahinian, P., Smith, H.,and Hawthorne, J., "Fatigue Crack Propagation in Stainless Steel Weldments at High Temperature," *Welding Research Supplement*, 527-32, 1972.
27. Bamford, W., "Fatigue Crack Growth of Stainless Steel Piping in a Pressurized Water Reactor Environment," *J. Pressure Vessel Technology, 101*, 73-79, 1979.
28. Pickard, A., Ritchie, R., and Knott, J. F., "Fatigue Crack Propagation in a Type 316 Stainless Steel Weldment," *Met. Technology 2*, 253-63, 1975.
29. Tang, S. S., *pc-CRACK Fracture Mechanics Software User's Manual*, provided by Structural Integrity Associates Inc., San Jose, California, 1989.
30. Kanninen, M. F. Mukherjee, A. K., Rosenfield, A. R., and Hahn, G. T., " The Speed of Ductile Crack Propagation and the Dynamics of Flow in Metals," *Symposium on Mechanical Behavior of Materials under Dynamic Loads*, San Antonio, 1967.
31. Duffy, A. R. et al., "Fracture Design Practices for Pressure Piping," Fracture V, pp. 159-232, Liebowitz ed., Academic Press, 1969.

Appendix A

Data Collection and Instrumentation Details

Data Collection

The data acquisition system consisted of four major parts: a centralized Hewlett Packard (HP) series 9000 UNIX workstation; an HP model 3565S signal analyzer; an HP model 700/RX x-terminal linked to the workstation through a building local network; and a Structural Dynamics Research Corporation (SDRC) software package which acquired, analyzed and displayed the experimental results. The workstation consisted of an HP model 375 computer with 32 Mbyte of memory, approximately 2 gigabytes of SCSI disk storage space, and a 1.3 gigabyte cassette magnetic tape drive for permanent storage. The operating system was HP-UX version 7.0. Several different plotters were employed on the network for hard copy displays. The HP 3565S multichannel measurement system is a computer-based system for signal acquisition and analysis and the measurement hardware is modular in design. The analyzer consisted of a 35650 mainframe, a 35651B interface/processor with 16 Mbyte of memory, a 35653A source module, and three 35655A 8-channel input modules, for a total of 24 input channels. The band width for the 35655A module is dc to 12.8KHz, with a dynamic range of 72dB. All 24 channels sample and hold simultaneously to maintain phase match across the channels. The input modules measure voltages with full scale input ranges from 5mV to 10V in 2dB steps and anti-alias protection on all ranges. The analyzer was linked to the workstation through IEEE-488 bus extenders (2 HP model 37204 extenders) and a 2-conductor glass fiber optic cable. The on-facility-site HP 700/RX terminal was linked to the HP-375 by an ethernet network which provided total support for data acquisition and display.

I-DEAS is a complete mechanical computer-aided engineering system which provides full function design, analysis, drafting and testing in a series of integrated modules with a common database and user-interface. I-DEAS Test Data Acquisition (p/n C03110) and I-DEAS Test Data Analysis (p/n 3070), version 5.0, are the software modules within I-DEAS which were purchased and used for the Pipe Impact Test Facility. These modules were specifically

configured to support the 3565S and its hardware modules in the HP-375 HP-UX environment. The 3565S is not fully supported by SDRC this results in some unsupported capabilities and operational limitations, but in general, these present only minor complications. Data acquired can be stored in the form of time histories and/or functions (e.g., frequency response functions, time-average, correlation matrix, auto spectra, and spectral matrix). These results can be easily accessed and displayed utilizing the sophisticated graphic features inherent in the I-DEAS package.

Instrumentation

The instrumentation used on the Impact Pipe Test Facility consists of standard, off-the-shelf products. Load (force) data were measured with an MTS model 661.23A-02 110 kip load cell. An MTS model 440.21 D.C. conditioner supplied excitation voltage and signal amplification. The actuator movement transducer, a linear variable differential transformer (LVDT), was supplied by MTS as an integral part of the actuator. An MTS model 440.22 A.C. conditioner and master oscillator supplied a 10KHz excitation carrier signal to the LVDT and an amplified VDC output signal. Both the load cell and LVDT were calibrated by MTS on site with secondary standards. Also, an MTS model 632.03E-30 crack-opening displacement (COD) gage was mounted across the initial 1-inch crack (see Fig. 28) during most of the test. A second 440.21 D.C. conditioner provided signal processing. The COD gage system (gage/cable/conditioner) was calibrated using an MTS model 650.03 calibration.

A total of 17 strain gages were installed on the pipe before test initiation (numbered XE-100 through XE-116). Their locations are shown in Fig. 28. Usually only seven of these gages were connected to the data acquisition system at a time, with the particular gage utilized depending on the crack extension. The gages were foil-type, 1/4-inch gage length, 350 OHMS and compensated for stainless steel [Micromeasurements (MM) part number WK-09-250BG-350 option SP30). The gages were bonded to the pipe with MM M-bond 610 epoxy-phenolic adhesive. MM model 2310 signal conditioner amplifiers provided bridge completion, 3.5 VDC excitation, and signal amplification. The standard quarter bridge, three wire, internal dummy gage configuration was used. Internal shunt calibration resistors provided signal calibration. The frequency response of the 2310 amplifier is stated as dc to 25KHz, -

0.5db in the D.C. coupled wide-band operational mode (as used for this test) at all gains and output levels.

Crack propagation gages provided a means of measuring crack extension during the test, especially during the dynamic impacts. Three different types of MM crack propagation gages were utilized; p/n TK-09-CPA01-005, TK-09-CPA02-005, and TK-09-CPC03-003 with a resolution (distance between wires) of 0.01 inch, 0.02 inch, and 0.08 inch, respectively. Pacific model 8210 bridge completion modules were used in the constant current mode to condition the gages. Before test initiation, each gage type was manually broken, wire by wire, to simulate crack extension and insure proper operation of the total gage system. Only step changes in the output signal were necessary to determine crack extension, thus the actual absolute output values were not critical. The gages were installed with MM M-bond-200 and with Devcon (stock no. 14250) 5-minute epoxy. Figure 28 shows the location of the first two gages. Subsequent gages were located at the crack tip as the crack extended.

Direct current displacement transducers (DCDT's) were used to sense the macroscopic bending of the pipe during all phases of the test. Three DCDT's (see Fig. 29, one on each end and one in the middle of the pipe) provided the data which was compensated for rigid body motion. TRANS-TEK model 354-000 transducers with ±1 in. ranges were used. MM 2310 signal conditioning amplifiers supplied 12VDC excitation and gain. The transducers were calibrated using a 1 in. micrometer. The nominal linearity for this DCDT is .010 inch over the total working range of 2,000 inches. The internal carrier frequency of these units was 3200HZ, which may explain their delayed/filtered response relative to the COD gage and the LVDT during the impact loadings.

The accelerometers used for this testing were PCB Piezotronic model 302A02 transducers. They are quartz accelerometers which utilize the ICP (Integrated Circuit Piozoelectric) instrumentation. Their nominal characteristics are; voltage sensitivity of 10mV/g, range of ±500g for ±5VDC, resolution of 0.01g, frequency range at ±5% of 1 to 5000 HZ or ±10% of 0.7 to 10KHZ, and temperature range of -100 to 175°F. A PCB mode 483B03 provided constant current excitation over the signal lead, decoupled the signal from the transducer D.C. bias, and provided a unity gain buffered output signal. Seven

accelerometers were mounted on the pipe at the locations shown in Fig. 29 (CE-100 through CE-107).

Miscellaneous equipment used for display and operation of the test were Keithley model 197 digital multimeters, SOLTEC model VP-62236 strip chart recorders, and flatbed x-y recorders (HP and MTS). Also, two Dorce trendicators (model 410A) provided manual temperature data from the 10 chromel-alumel (type K) thermocouples. Six thermocouples were distributed along the pipe length and around the pipe circumference to assess the temperature distribution of the pipe as a structure. Four thermocouples were mounted 4 in. from the center of the initial crack in the axial and circumferential directions. These circumferential thermocouples were relocated after the crack extended beyond their original locations.

An MTS model 810 servo-hydraulic close-loop control system was used to subject the pipe to the conformance loadings, fatigue cycles for crack extension and crack sharpening, and for the static pre-load during the dynamic impacts. This system was based on two 442 controllers, but consisted of a 413 master control panel, 410 digital function generator and a 417 cycle counter. The system controlled an MTS model 204.81 110 kip actuator in load or stroke control through an MTS model 294.12 service manifold.

Figure 13 provides a photograph of the fully instrumented central pipe section.

APPENDIX B

Fatigue Crack Growth Methods

The effect of various parameters on the fatigue crack propagation behavior of a 316 stainless steel weld defect needs to be considered to complete a fatigue crack-growth analysis. Applicable fatigue crack-growth data and parameters such as environment, frequency, stress-intensity factor threshold, residual stress, and crack retardation were investigated.

The fatigue crack-growth analysis of a 316 stainless steel weld defect requires compilation of fatigue crack-growth data in an NPR-HWR environment. A data base of crack-growth results for 316 stainless steel product forms in air and PWR environments was compiled with assistance from the Battelle/EPRI data base management system, EDEAC [22]. Fatigue crack propagation rates for 316 stainless steels differ from those of other austenitic stainless steels under similar conditions [23]; therefore, only 316 stainless steel plate, casting, and weldment data were utilized. Figure 7 shows weldment, casting, and plate data separated by material form [24-26]. Growth rates in austenitic stainless steel weldments are generally equivalent to or lower than growth rates in wrought stainless steels; therefore, all 316 stainless steel product forms were included in the analyzed data base [27]. A statistical regression was performed to determine the parameters C and n for the equation $da/dn = C(\Delta K_{eff})^n$ [21]. Figure 7 also shows a graphical upper bound to the data and its corresponding C and n parameters. Because the NPR-HWR environment has a higher oxygen content than PWR environments, the Upper-Bound Crack Growth Rate curve was used in the analysis to be conservative. Tests currently being completed at Argonne National Laboratory on Type 316NG in simulated NPR-HWR environment and temperature [12] do show this to be conservative (see Fig. 7).

The fatigue crack-growth rate data are plotted as a function of K_{eff} in Fig. 7. As described K_{eff} is a function of the stress-intensity factor ΔK and the cyclic stress ratio R. The R ratios of the compiled 316 stainless steel data were to ≤ 0.2; thus, one plot (Fig. 7) of da/dN vs K_{eff} was utilized for the data, where K_{eff} was in the form of a Walker relationship.

A variety of parameters affect the fatigue crack propagation rates of austenitic stainless steels. These parameters include environment, frequency, stress intensity threshold, residual stresses, crack retardation, and stress-intensity ratio (R).

Temperature and environment can have a profound effect on fatigue crack growth. As mentioned previously, both air and PWR environments were included in the data base. Reference 17 indicated a negligible difference between air and PWR environment. The temperature range chosen was 260 to 427°C (500 to 800°F), which encompasses the NPR-HWR reactor operating temperature of 110°C (230°F) and is conservative. The effect of frequency has been assumed to be negligible at these temperatures [27].

A large number of cycles at very low stresses can result in crack growth to a critical flaw size within the design life of the reactor if there is no stress-intensity factor threshold. For this reason, calculations did not include a stress-intensity factor threshold. A threshold value for 316 stainless steel welds in a NPR-HWR environment has not yet been determined, but there are published values for stainless steels in air environments [28]. Threshold values of 4.6 ksi $\sqrt{in.}$ and 2.6 ksi $\sqrt{in.}$ have been identified but were not used in this analysis because the minimum loading values are above the threshold.

There are currently no generally accepted means for taking crack retardation into account. Crack retardation occurs when a high cyclic stress blunts the crack tip and causes less crack growth to occur until the crack grows out of the blunted crack stress field. Ignoring crack retardation is conservative, and this approach was taken in the analyses.

In a crack-growth analysis, a stress-intensity factor range ΔK must be calculated. This calculation is dependent on an existing time-dependent axial stress distribution for each of the transients discussed earlier. This time dependence is primarily due to the thermal stress component of the total axial stress distribution. A thermal analysis was first performed to determine the temperature gradients for the piping wall location of concern for all transients considered.

APPENDIX C

Fracture Mechanics Analysis

A fracture mechanics analysis of the test pipe conditions was completed in order to estimate the tearing instability point and flaw size. For this analysis, an estimation scheme for J was used as follows:

$$J = \frac{\pi \sigma^2 a}{E} + 2.67\pi a \sigma \epsilon_{PL}$$

where:

σ is bending stress in the pipe (psi).

a is half the crack length in inches.

ϵ_{PL} is plastic strain from estimated stress vs strain curve.

E is 28,000,000 psi.

The resultant J for 1 SSE loading as a function of half crack length is shown on Fig. 30.

Using the above relationship for J, the tearing modulus T was calculated for various crack sizes. This relationship is shown on Fig. 31. A review of published data on stainless steel 316L provided a minimum tearing modulus (Tmat) for weld metal of approximately 100. This value was used to estimate the tearing instability crack size as shown on Fig. 31. This resultant instability crack was a = 7 in. or total flaw length of 14 in.

Figure 32 provides an estimate of J_{IC} based upon the ORNL pipe tests. The J value was estimated using the crack opening displacement (COD) measurement and the pipe loading value. The COD was reduced based on geometry relationships of the pipe bending at various crack sizes. This reduced plastic COD was then added to a calculated value of elastic crack opening as follows:

$$\delta = \delta_{el} + F_{pl}\ (COD)$$

$$J = \delta\ \sigma_{ys}$$

The weld material yield stress σ_{ys} was estimated to be approximately 52,000 psi. The resultant estimate of J_{IC} of 3,400 in.-lb/in.^{2} is a reasonable value based on other investigators data. These calculational values will be compared to actual compact tension specimen data when it is available.

Figure 27 shows a sketch of the crack tip and plastic zone that was seen on testing completed December 20, 1991. This test was for a 7.6 in. long flaw and was loaded to 50,000 lb in bending. The crack tip did extend 0.02 in., but only after significant crack blunting. Loading to 55,000 lb then extended the crack by 0.10 in. and these values were used in estimation of J_{IC} as provided on Fig. 32 and discussed above. This initial crack extension followed the plastic zone a shown on Fig. 27.

APPENDIX D

Pipe Modal Analysis

Basic understanding of the important system modes of vibration is essential to understanding the phenomena during the impact testing. The breathing and bending modes of the pipe are the most likely contributors to crack propagation and structural responses of the pipe. For these reasons preliminary closed form calculation and a model survey were conducted to determine these frequencies of the pipe with and without the water present. The results were also correlated with the response measurements during the main impact event.

Modal frequencies were computed for simply-supported cylindrical shells without axial constraint and dry, i.e. no water in the pipe. These closed-form calculated values are shown in Table 1.D for the 3 and 8 foot sections using the Flügge method.* The 3 foot section represents the pipe span for the center section that is supported by the clamps on the loading frame (see Fig. 29). The simply supported approximation is not completely accurate for either the 3 foot or the 8 foot lengths since the pipe is continuous through the center supports and has some moment carrying capability at the ends due to the end caps. However, clamped end conditions are also not completely accurate so the simply supported was adopted due to the simplified calculations.

The modal survey was conducted using a small instrumented hammer to tap on the pipe near the quad CE102 and the center CE105 accelerometer locations. Frequency response functions were developed and modal frequencies were extracted from these response functions. Since the impact was localized and small in amplitude, the predominant excitation was for the pipe breathing modes. Other system modes such as the pipe bending mode were not excited. However, the beam mode is excited during the main impact event and correlates well with the calculated 10 Hz first bending mode of the 19 foot pipe. Table 1.D shows the

*Robert D. Blevins, Formulas and Natural Frequency and Mode Shape, Robert E. Krieger Publishing Co., 1987, page 302, Eqs. 12-18.

modal frequencies obtained using the "search peaks" algorithm of the SDRC-TDAS* software. These modal frequencies were also observed from the auto spectrums of each response measurement and in most cases from the time history response during ring down of the modal survey test.

Comparison of the closed-form solution and the modal survey test shows that the assumed boundary conditions are more important for the short 3 foot section at the center of the pipe than the longer 8 foot section containing the quad points. At the center of the pipe the calculated values underestimates the fundamental and higher order breathing modes of the pipe. For the 8 foot span the calculated frequencies are much more accurate due to the reduced effects of the boundary conditions.

The addition of water to the system was expected to reduce the frequencies and is so indicated by comparison of Table 1.D and 2.D. The closed form predicts that the added mass reduction in frequency is of the order of about 29% so that the calculated values in Table 2.D are 0.71 times the values in Table 1.D. Similar reductions were noted in the measured values for both the center and quad points. Again the length of the span of 3 foot verses 8 foot results in a considerable increase in frequency.

Response measurements in the center of the pipe contained a large frequency content in or around the 500 Hz region. As can be seen from Table 2.D the measured modal response of 482 Hz indicates that this response is the first pipe breathing mode. The response spectra of the crack opening displacement gage (COD), the accelerometers and the pressure measurement all showed large components in the 500 Hz region based on results from hit 6-0. The strain gage data (XE112) did not show a significant amount of the 500 Hz content. Also the accelerometer on the loading frame mount (CE107) did not show much 500 Hz content since it was not attached directly to the pipe. It should be noted that the frequency response functions for all these responses clearly indicated the presence of the first

*Structural Dynamics Research Corporation—Test Data Analysis System is a commercial software package being used for modal analysis at ORNL.

beam bending mode in the neighborhood of 10 Hz. The COD and the strain gages displayed the first beam bending very predominantly in the time and frequency domain.

Response of the quad accelerometers are about half the amplitude of the center accelerometers. Neither the 150 nor the 430 Hz modes showed up from the time or spectral plots of the quad points as expected from Table 2.D. In fact, the small response that was present seemed to be in 200 to 250 Hz range. Certain segments of the time history plots shows considerable 250 Hz where as the frequency response functions shows 150 to 200 Hz. In either case the quad breathing response is much lower amplitude and less important than the response near the center point.

Considering that the closed-form solution contained rather gross approximations regarding the boundary conditions, the comparison with the modal test results was reasonably good. For improved correlation a three dimensional finite element shell model of the pipe must be constructed that could accurately model the boundary conditions and the inherent coupling between the 3 foot and 8 foot sections. These system modes would provide a better understanding of the pipe dynamics and could be used to improve instrumentation location and sensitivities.

Table 1.D. Dry Modal Test Results

	Center of Pipe			Quad Points		
	CALC	2 Hits		CALC	5 Hits	
	L = 3 ft	CE105	CE106	L = 8 ft	CE104	CE102
1	402.	596.	608.	231.	205.	204.
2	642.	1074.	1086.	596.	538.	536.
3	1147.	1725.	1718.	1114.	1258.	1073.
4	1810.	—	—	1779.	1674.	1678.

Table 2.D. Wet Modal Test Results

	Center of Pipe			Quad Points		
	CALC*	4 Hits		CALC*		
	L = 3 ft	CE105	CE106	L = 8 ft	CE104	CE102
1	285.	483.	482.	154.	156.	158.
2	455.	949.	949.	423.	432.	428.
3	814.	1441.	1439.	791.	984.	983.
4	1285.	—	—	1263.	—	—

*CALC for wet taken as = 0.71 (f_{Dry})

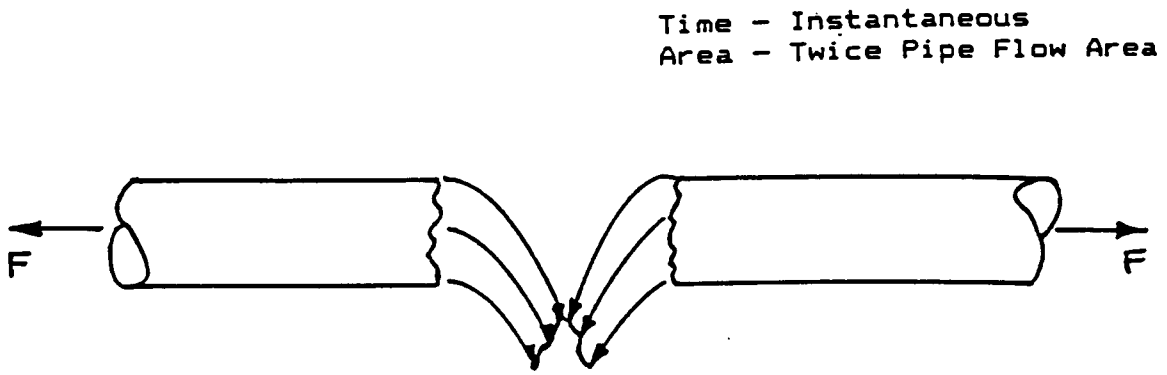

Fig. 1. Double-Ended-Guillotine-Break

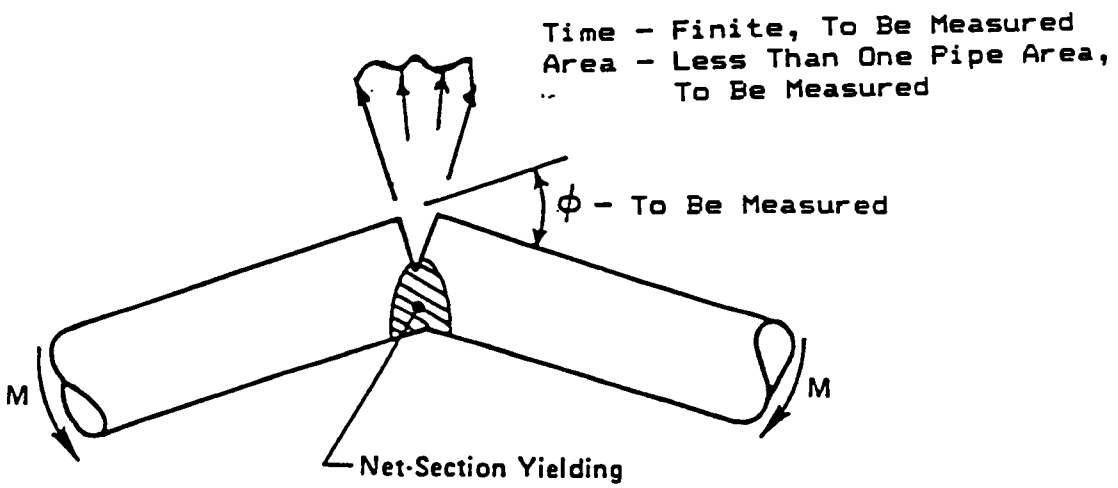

Fig. 2. Failure of Circumferentially Cracked Pipe Under Seismic Loading

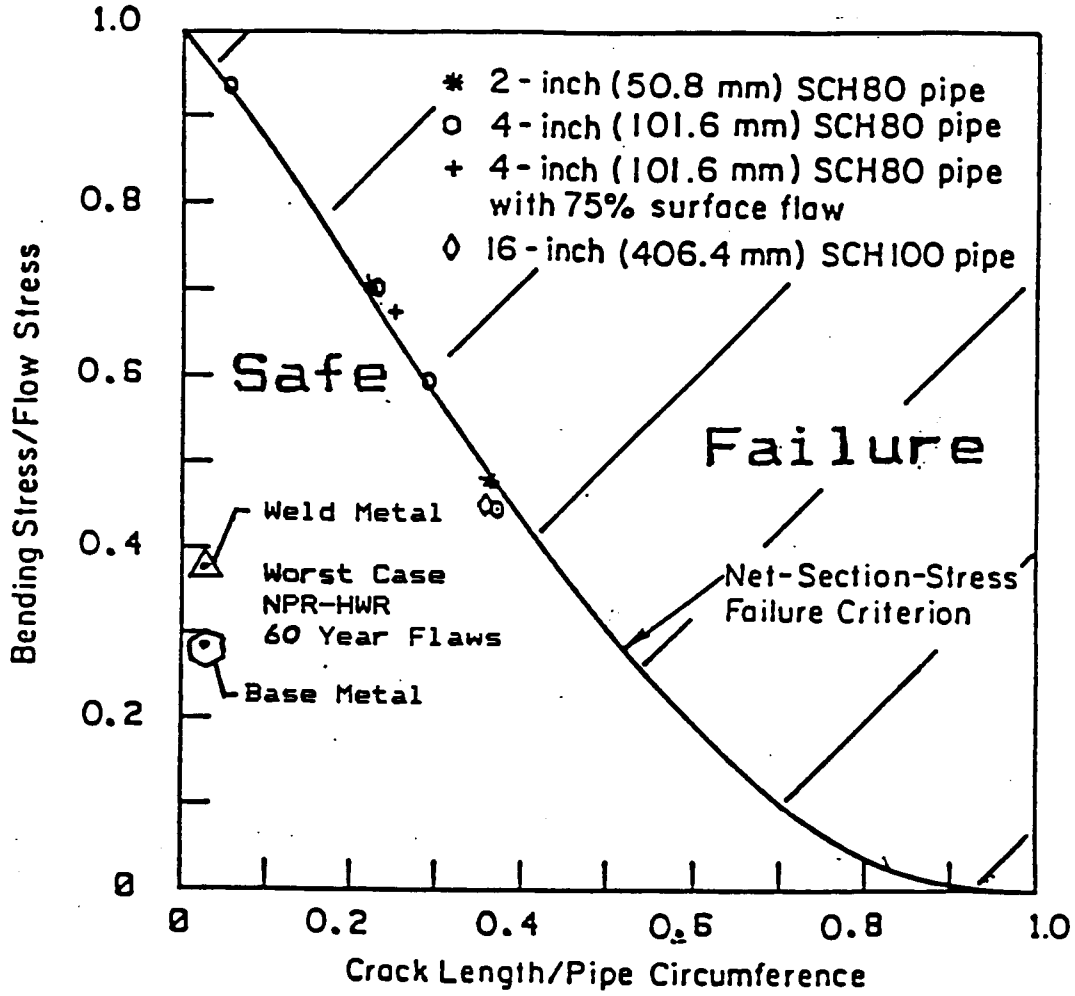

Fig. 3. Comparison of Net-Section Collapse Criteria With Pure Bending Data on Stainless Steel Pipes with Through-Wall Flaws

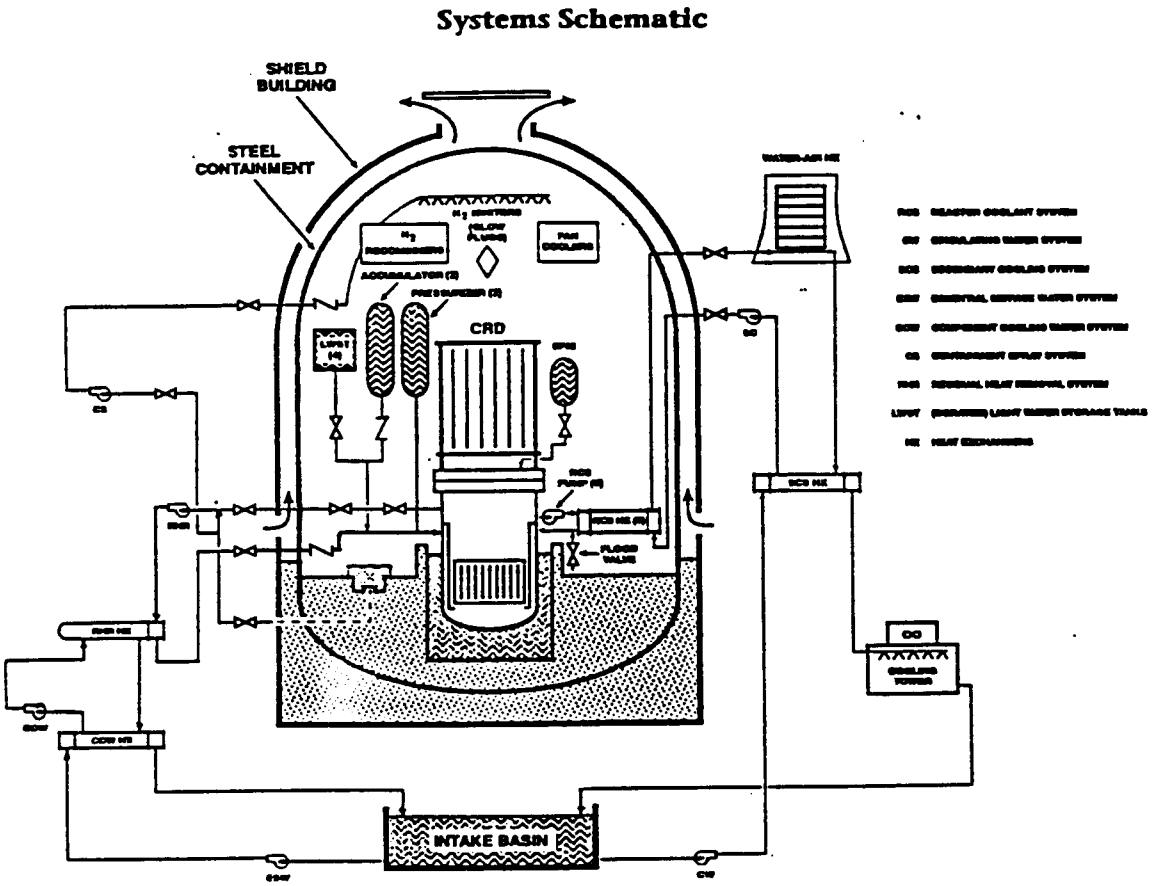

Fig. 4. NPR-HWR Plant

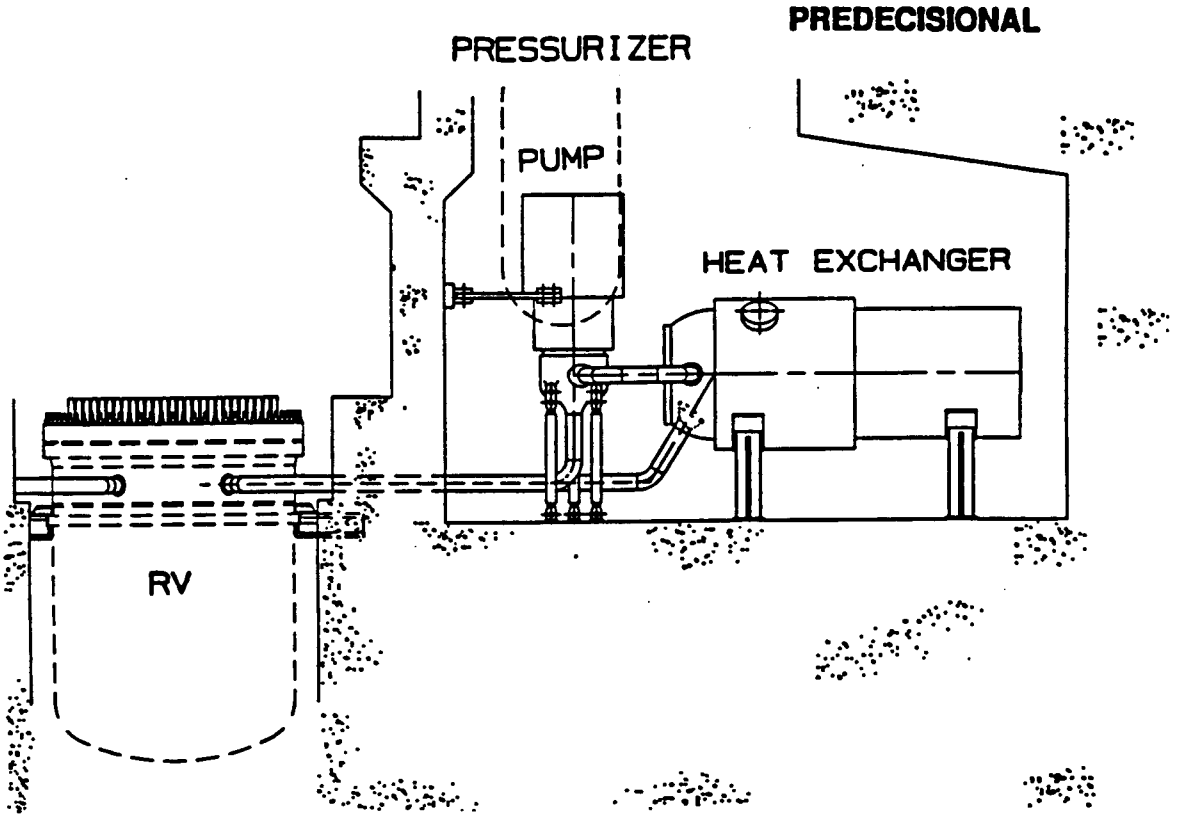

Fig. 5. RCS-1 of 6 Loops Elevation View

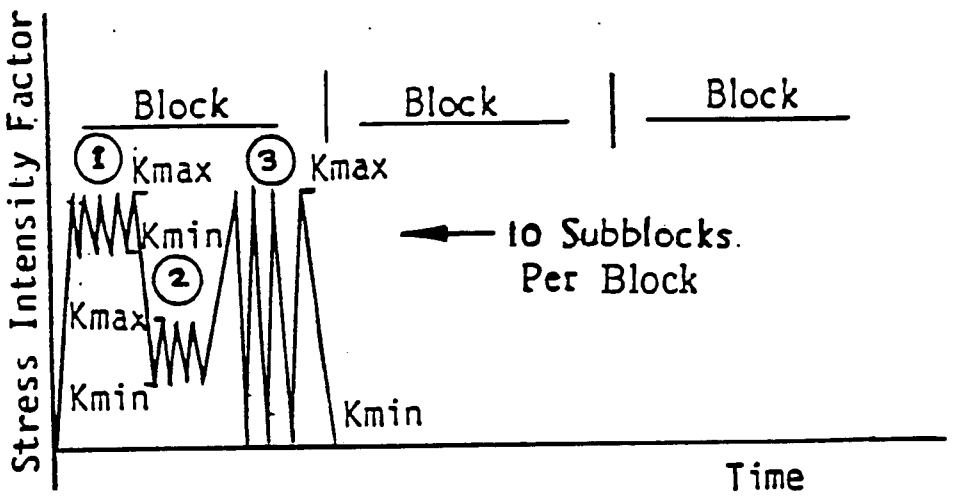

Fig. 6. Definition of Blocks and Subblocks for Fatigue Cycling

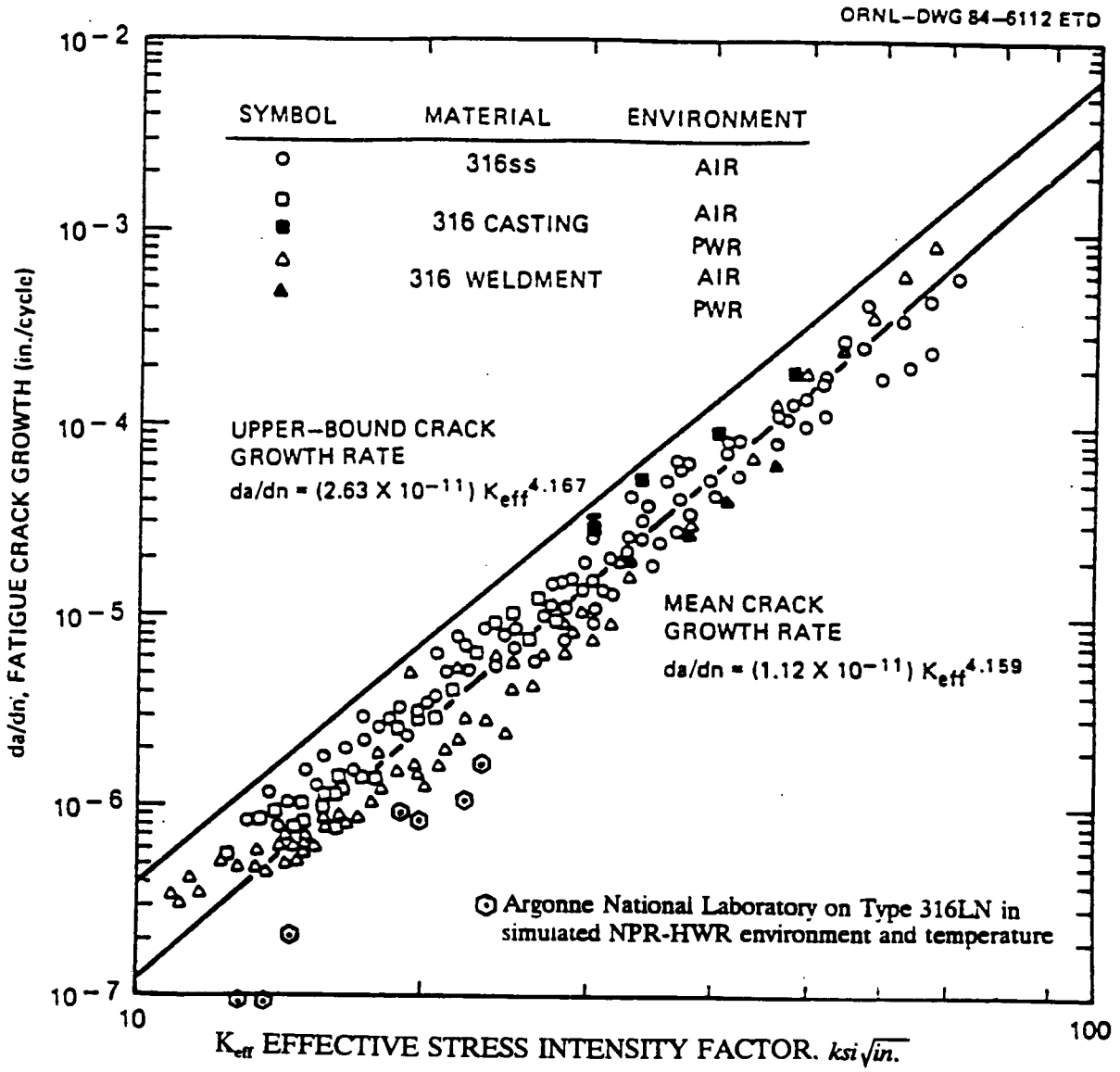

$$K_{eff} = K_{max}\,(1-R)^{0.5}\left[KSI\sqrt{IN}\right]$$

1 $ksi\sqrt{in}$ = 1.1 $MPa\sqrt{m}$

1 in./cycle = .0254 m/cycle

Fig. 7. Crack Growth Rate Versus Stress Intensity

Semi–Circular Crack in Half Space

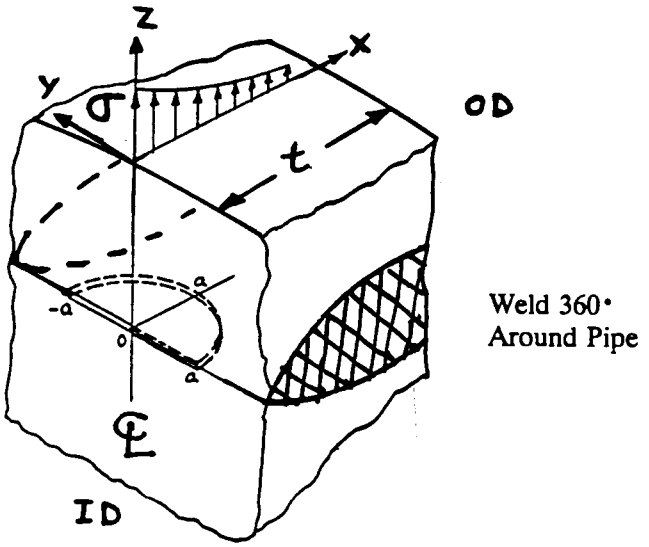

Weld 360°
Around Pipe

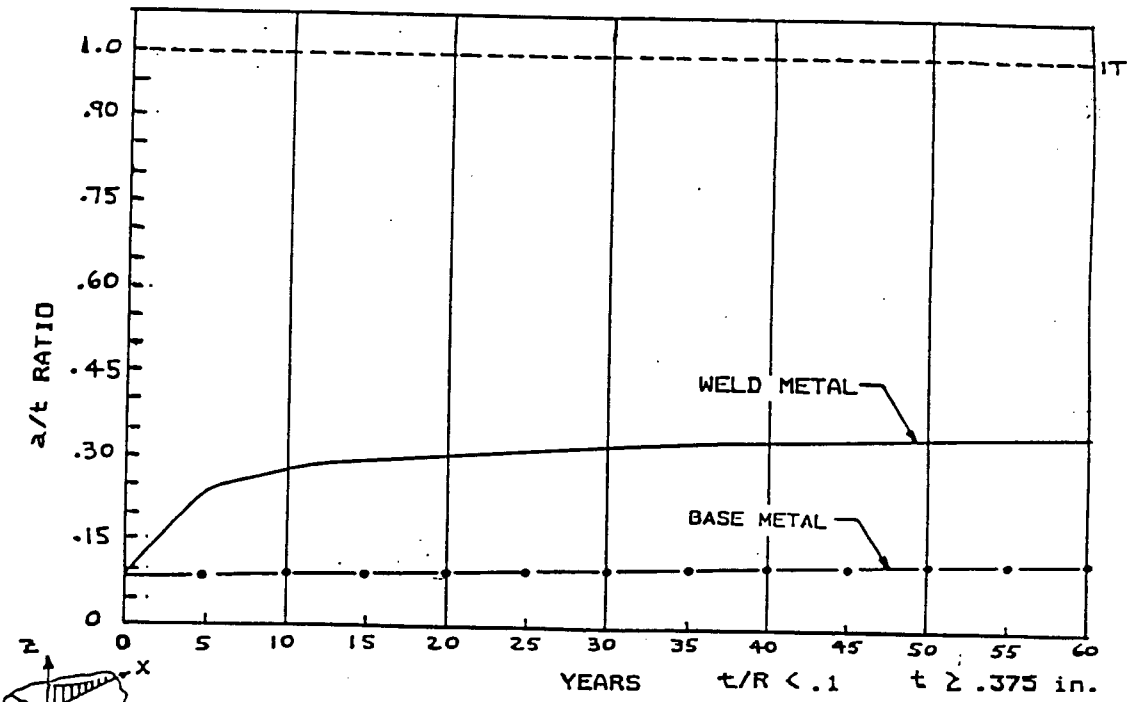

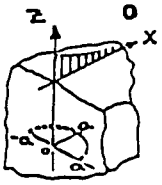

LEFM Crack Model J — Semi–Circular Crack in Half Space

Fig. 8. 16-Inch Diameter Pipe/Schedule 40/Crack Growth for 60 Years

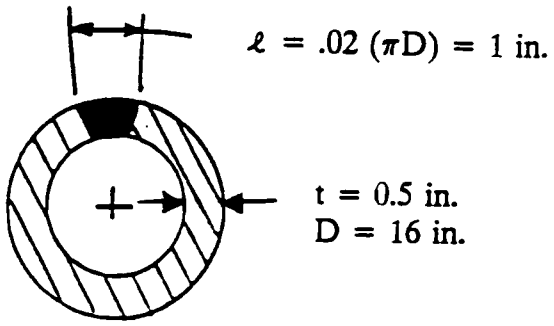

Base Material Flaw

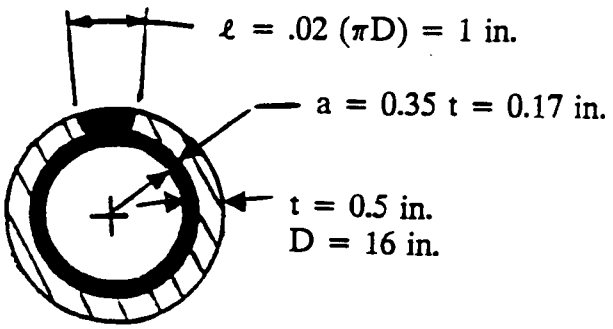

Weld Metal Flaw

Fig. 9. Worst Case Degraded Pipe 60 years

Photo 8498-91

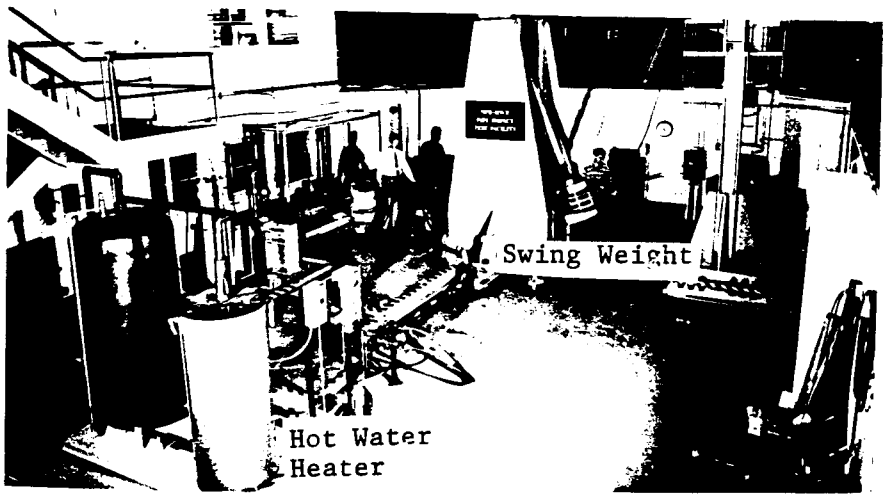

Fig. 10. Pipe Impact Test Facility at ORNL

Photo 8500-91

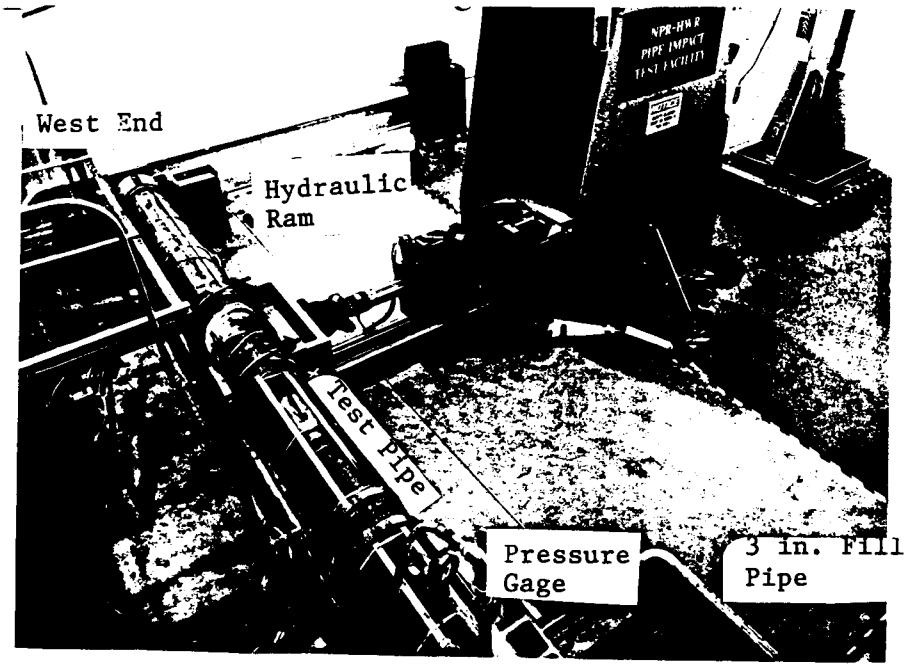

Fig. 11. Pipe Impact Test Facility at ORNL

Photo 8496-91

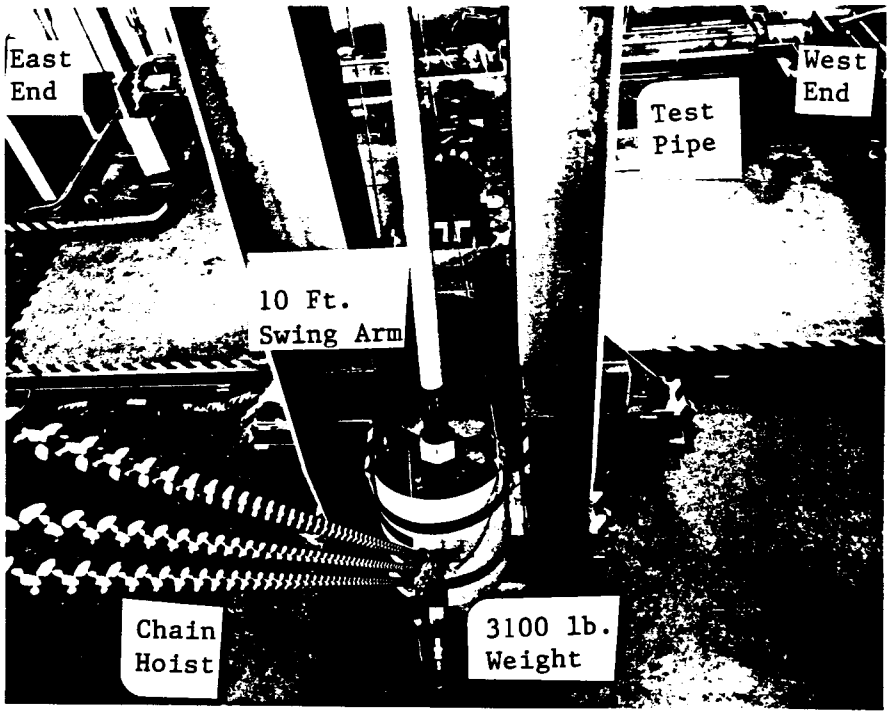

Fig. 12. Pipe Impact Test Facility at ORNL

Photo 8494-91

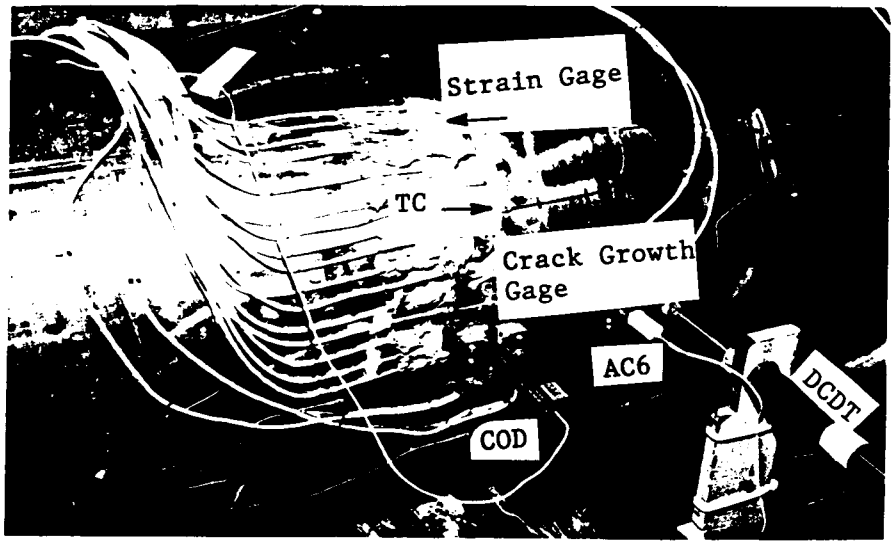

Fig. 13. Pipe Test Specimen at ORNL

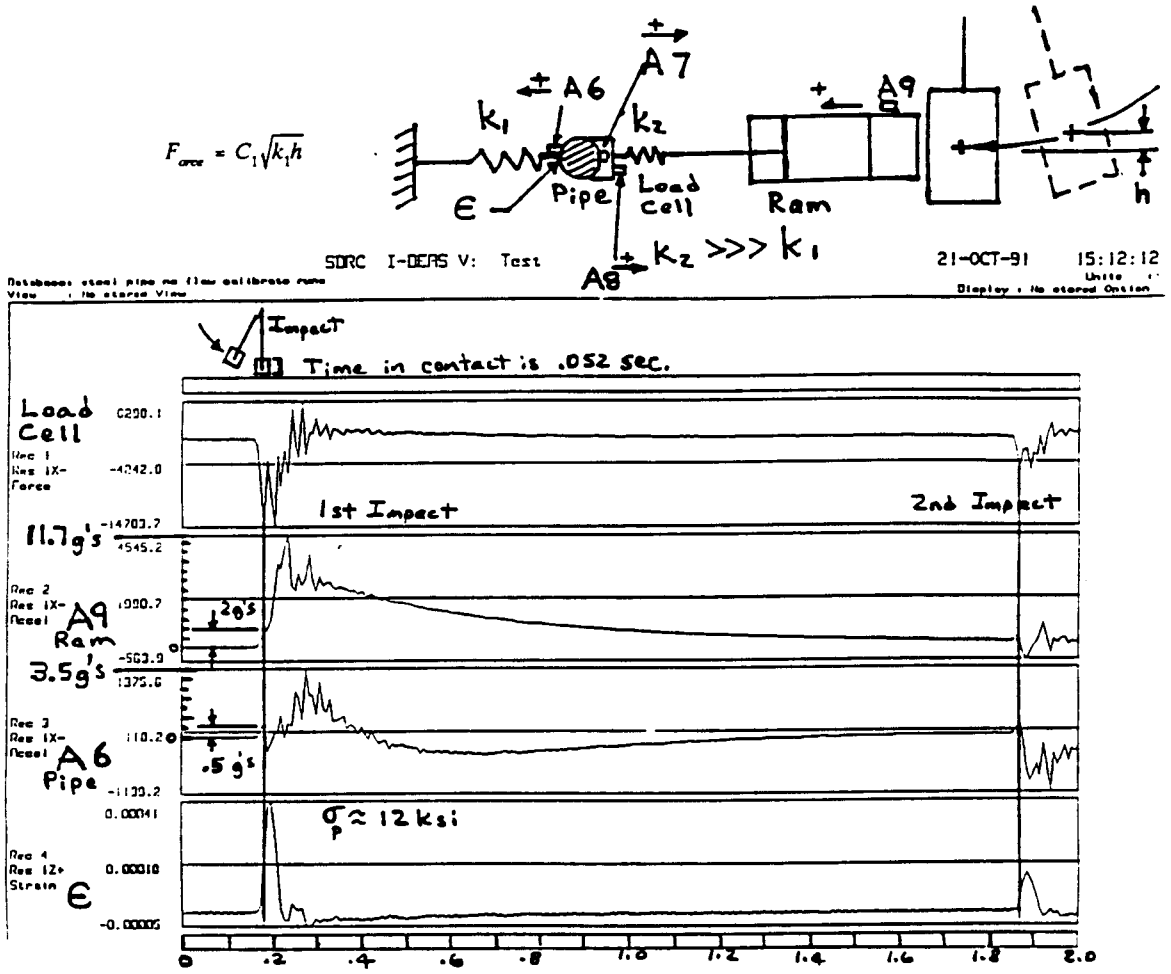

Time ~ seconds

Fig. 14. Data Collection Method

LOAD
vs
TIME

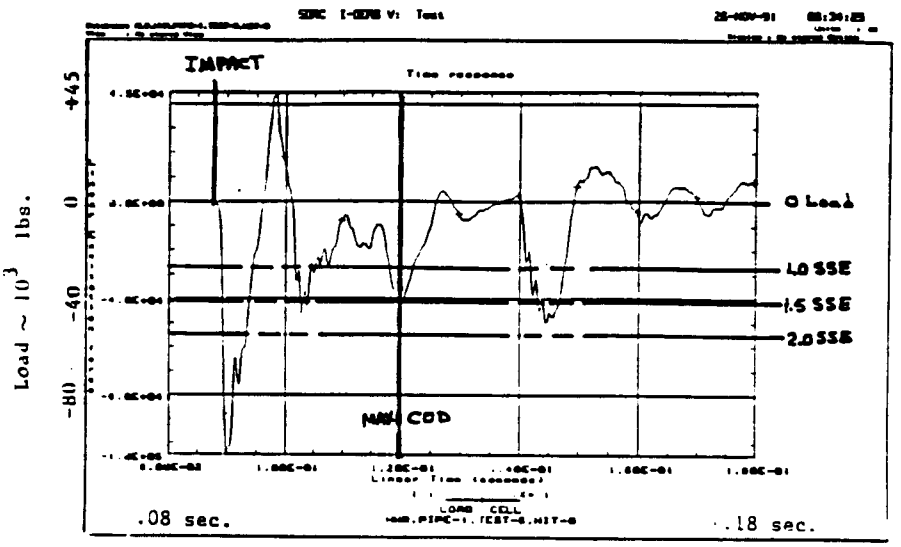

Fig. 15. Load Versus Time

DEFLECTION
vs
TIME

Damping = ξ = .11

f ≈ 20 Hz

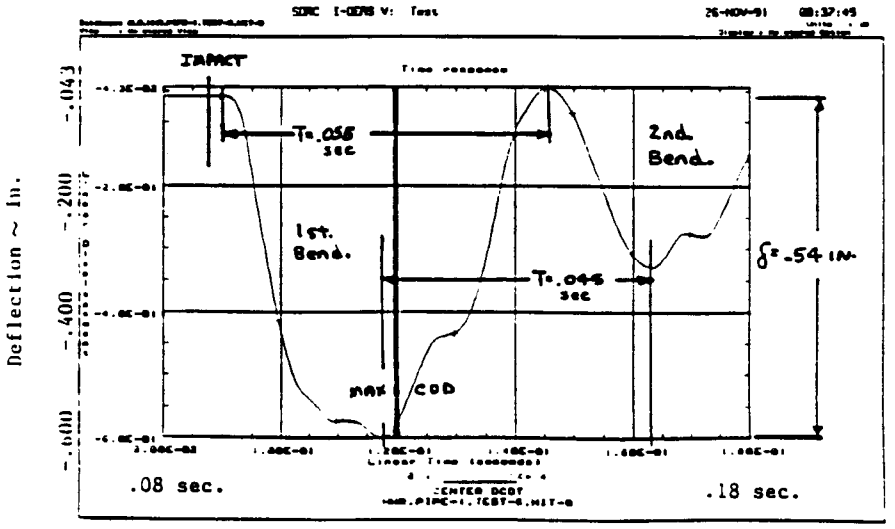

Fig. 16. Deflection Versus Time

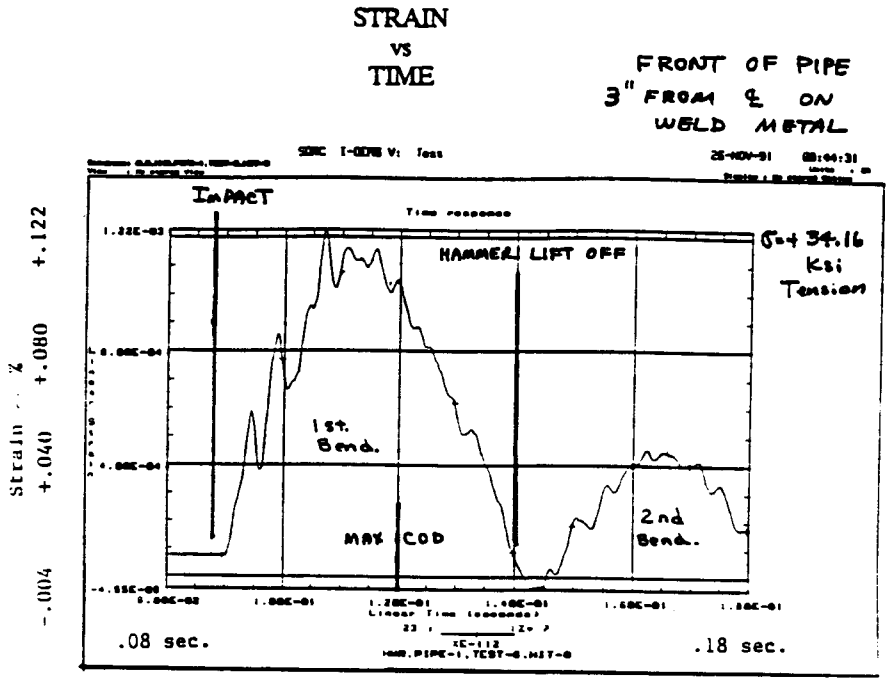

Fig. 17. Weld Metal Strain Versus Time

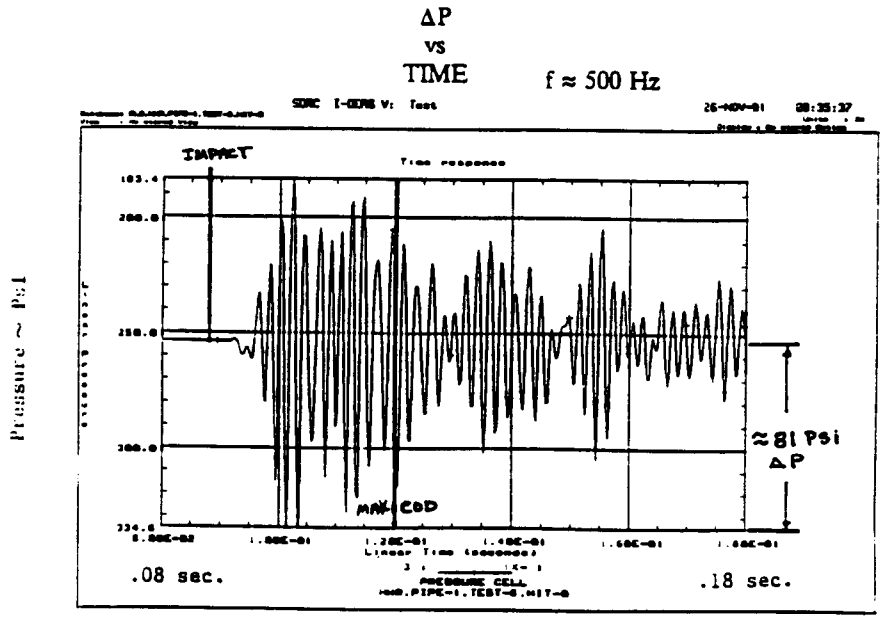

Fig. 18. Pressure Versus Time

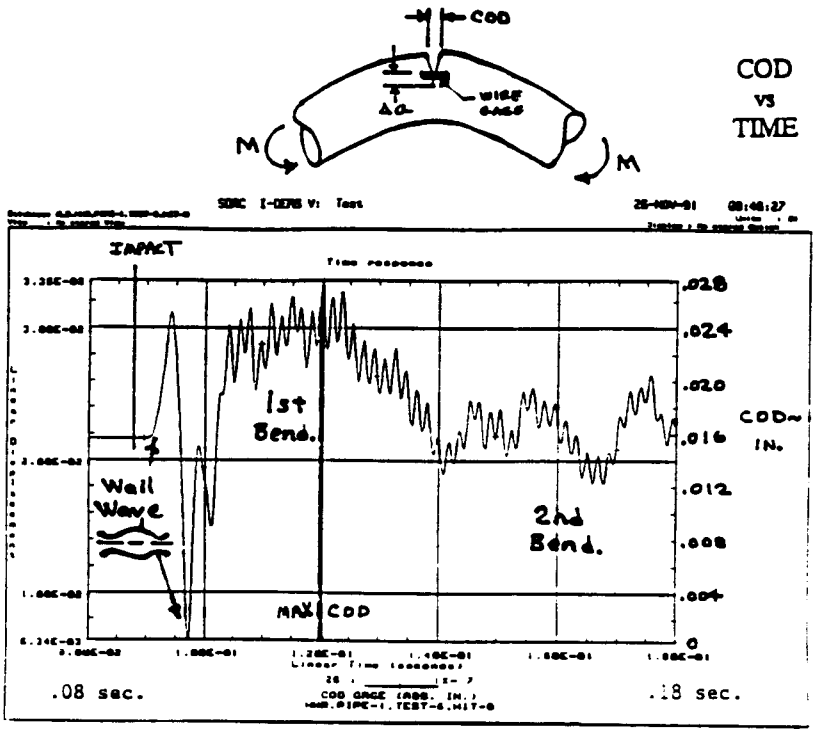

Fig. 19. Crack Opening Versus Time

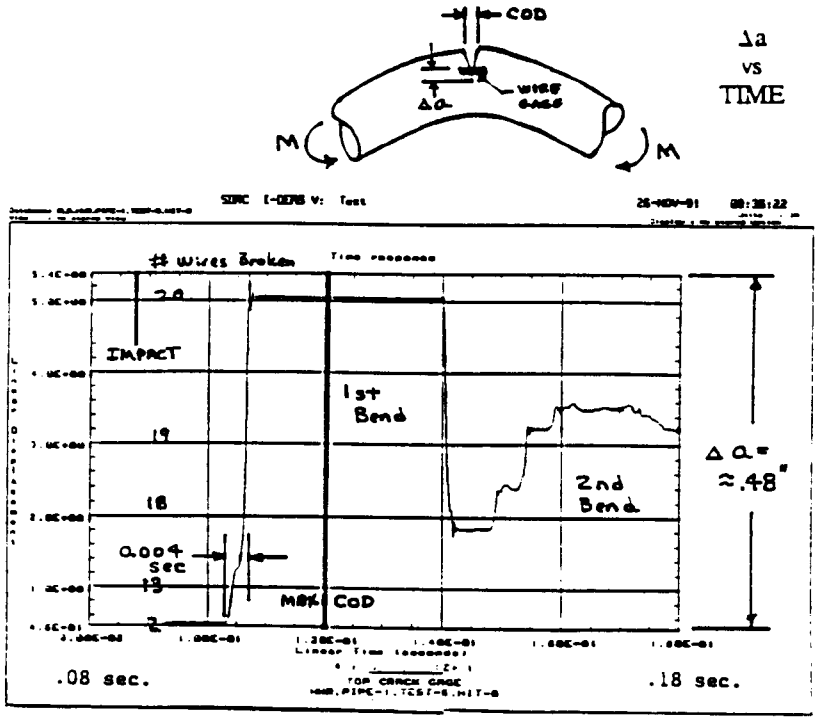

Fig. 20. Crack Growth Versus Time

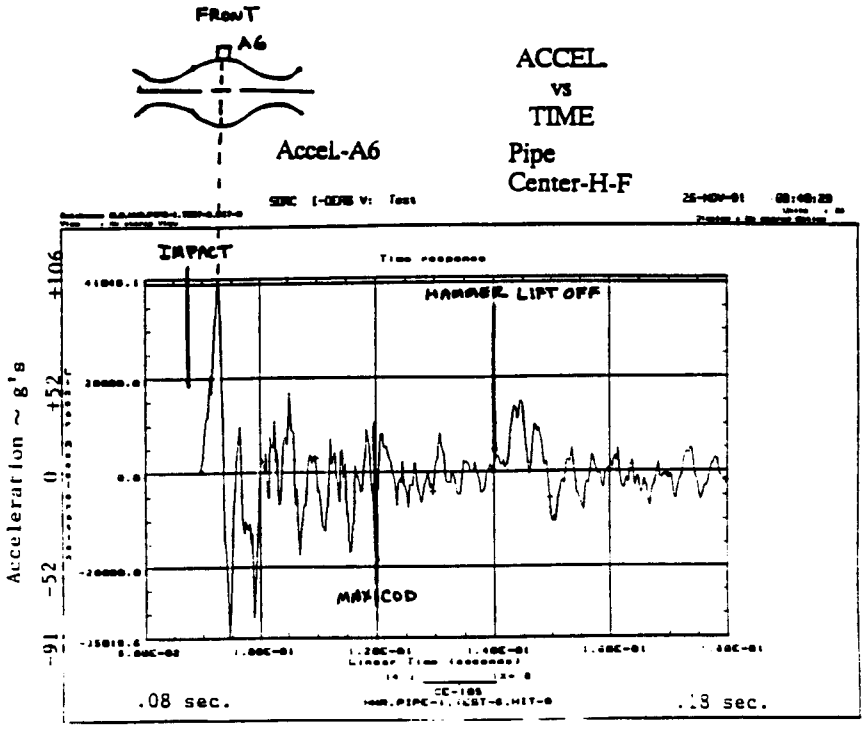

Fig. 21. Accelerometer A6 Versus Time

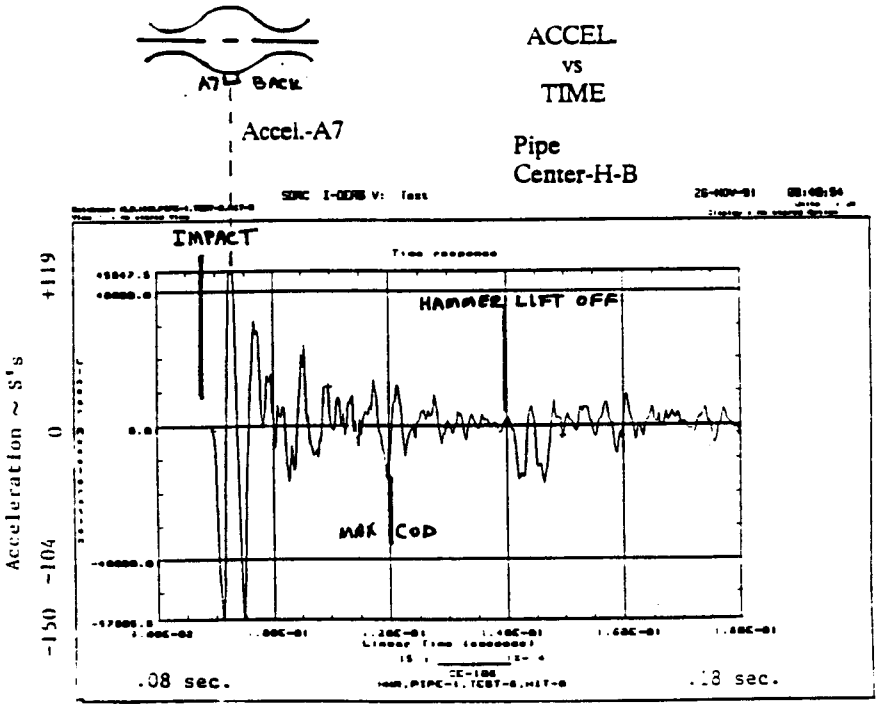

Fig. 22. Accelerometer A7 Versus Time

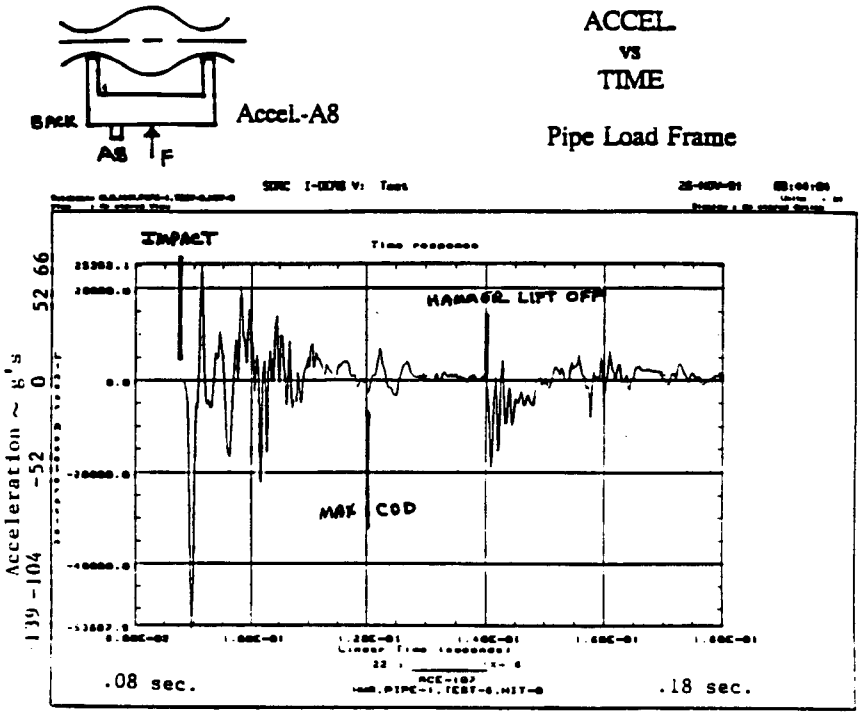

Fig. 23. Accelerometer A8 Versus Time

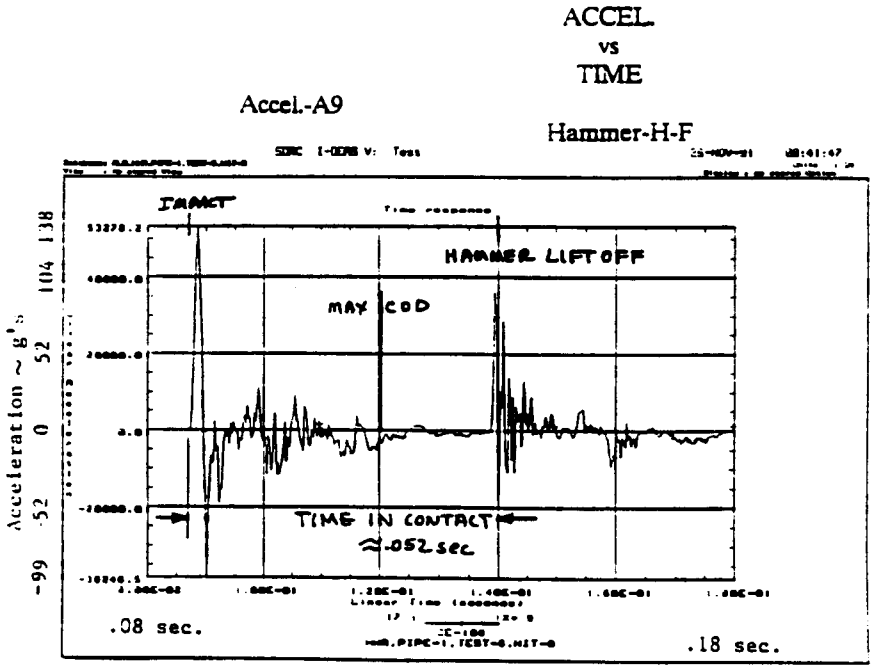

Fig. 24. Accelerometer A9 Versus Time

FLOW RATE
vs
CRACK SIZE

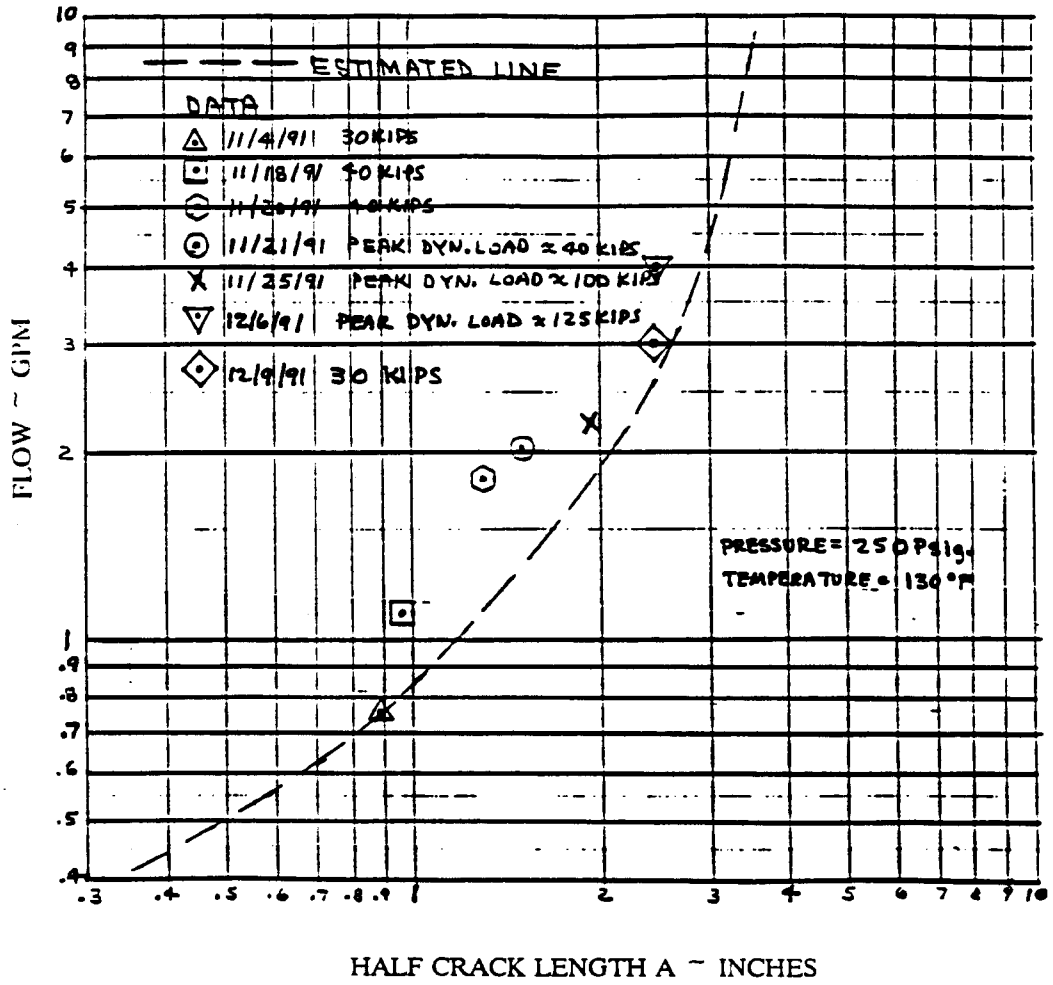

Fig. 25. Flow Rate Out of Crack Versus Length of Crack

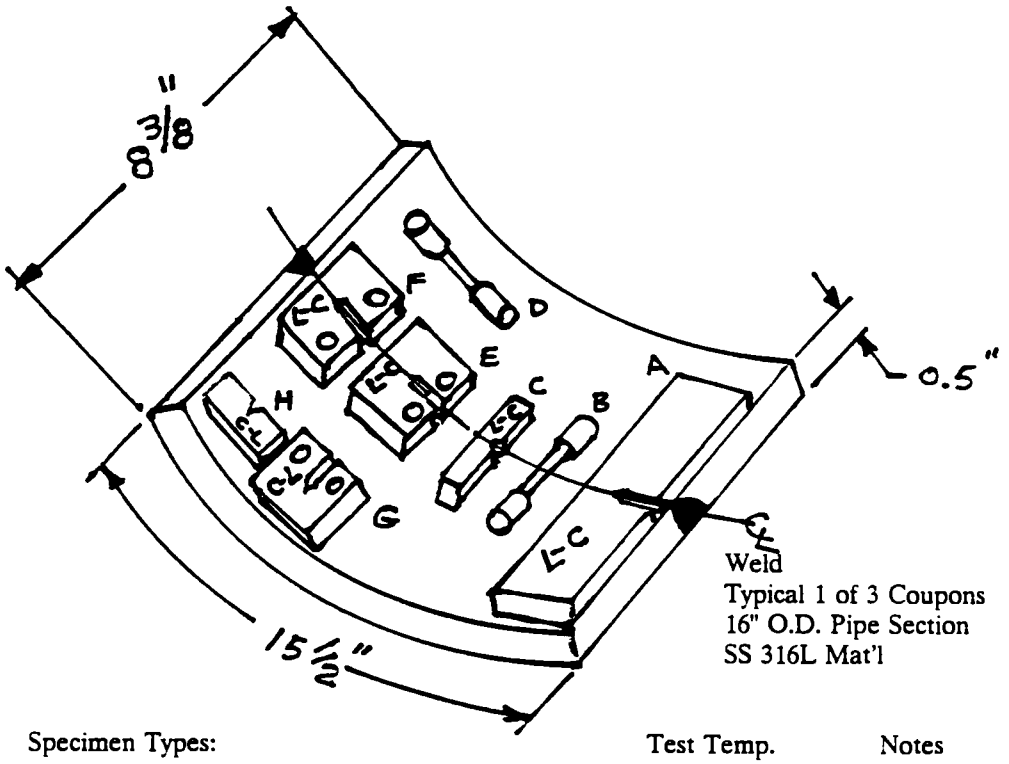

Specimen Types:		Test Temp.	Notes
A Bend—SE (B)	L-C Orientation	140°F	(1)
B Tension—T	Axial Orientation	140°F	(1) (2)
C Charpy V-notch CVN	L-C Orientation	140°F	(1)
D Tension—T	Circ. Orientation	140°F	(3) (2)
E Compact (tension) C (T)	L-C Orientation	140°F	(1)
F Compact (tension) C (T)	L-C Orientation	230°F	(1)
G Compact (tension) C (T)	C-L Orientation	140°F	(3)
H Charpy V-notch CVN	C-L Orientation	140°F	(3)

(1) The 2nd and 3rd coupons should center notch on HAZ and Base Metal respectively.
(2) Provide True Stress—True Strain curve.
(3) The 2nd and 3rd coupons should be tested at 75°F and 230°F respectively.

Fig. 26 Material Specimens from Pipe Coupons

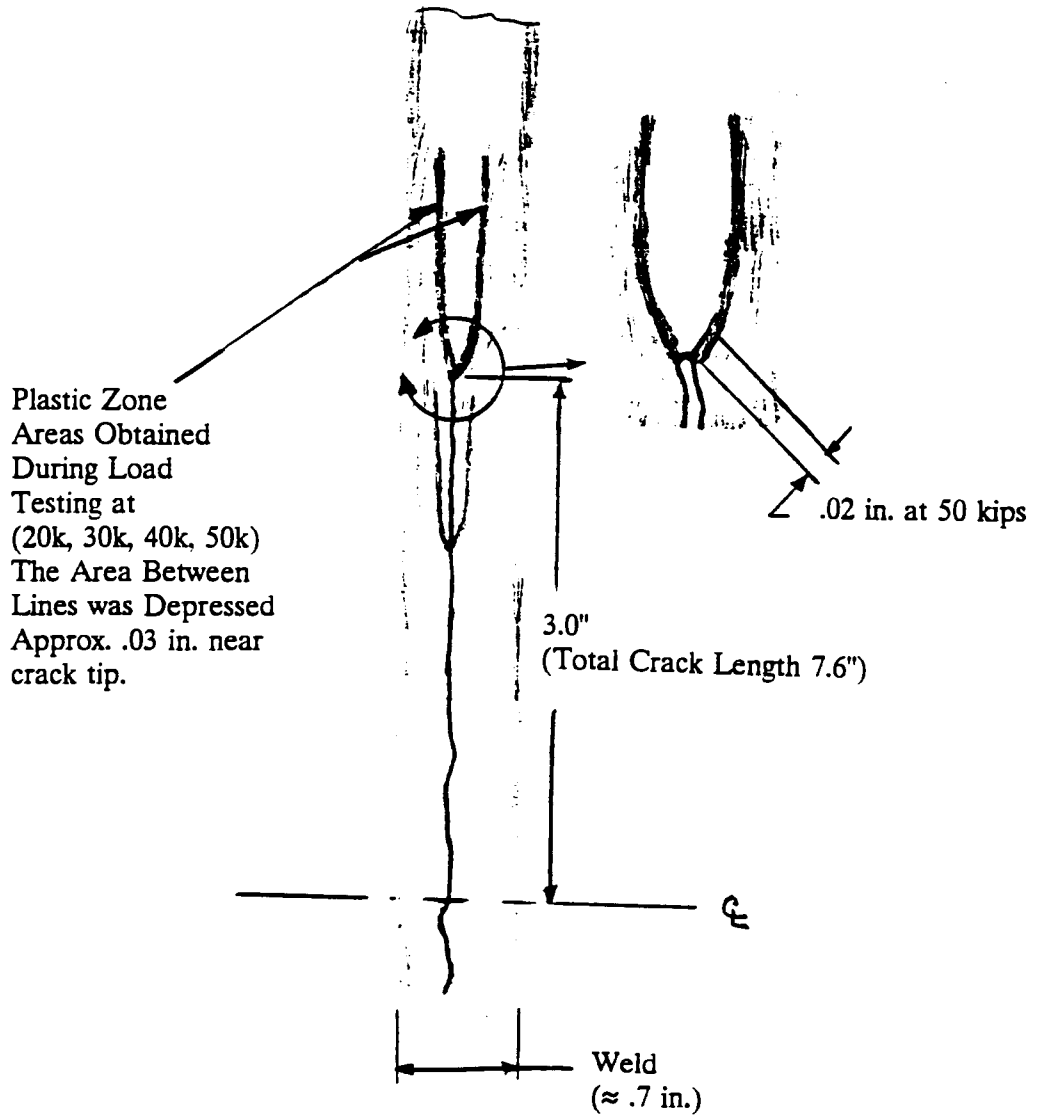

Fig. 27. Crack Extension and Plastic Zone Deformation During Compliance Loading (December 20, 1991)

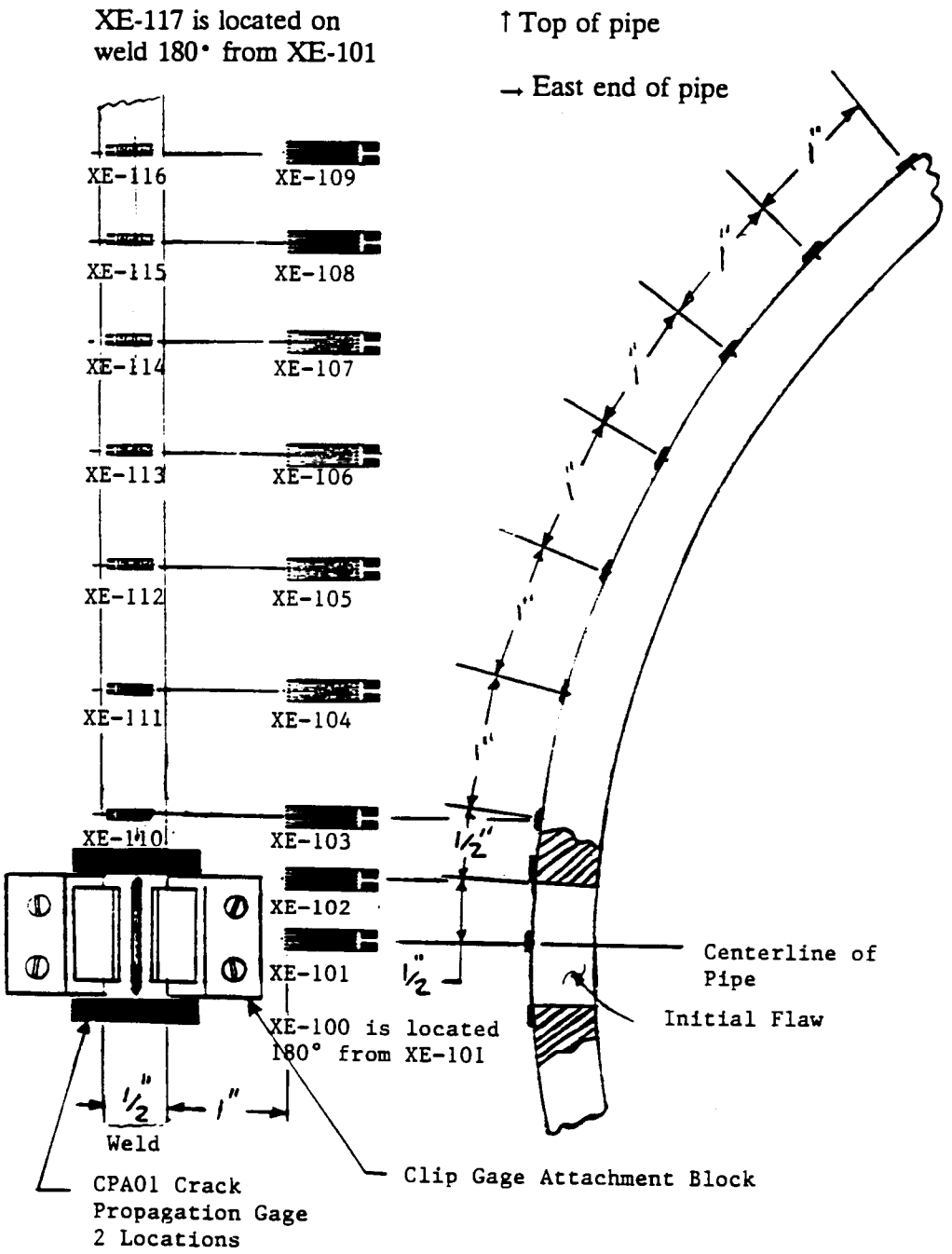

Fig. 28. Strain Gage and Crack Propagation Gages Located on Pipe

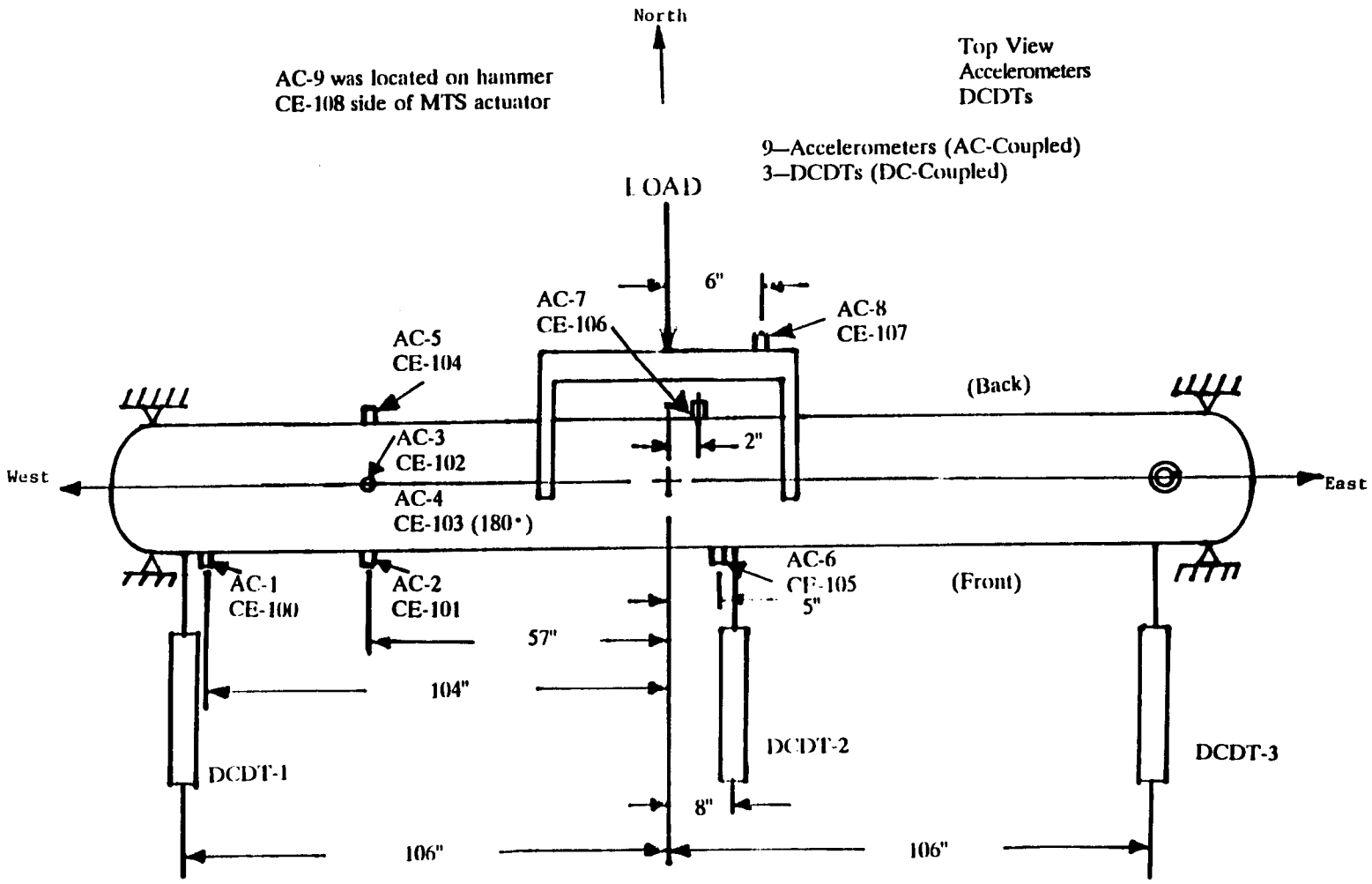

Fig. 29. Location of Accelerometers and DCDTs on Pipe

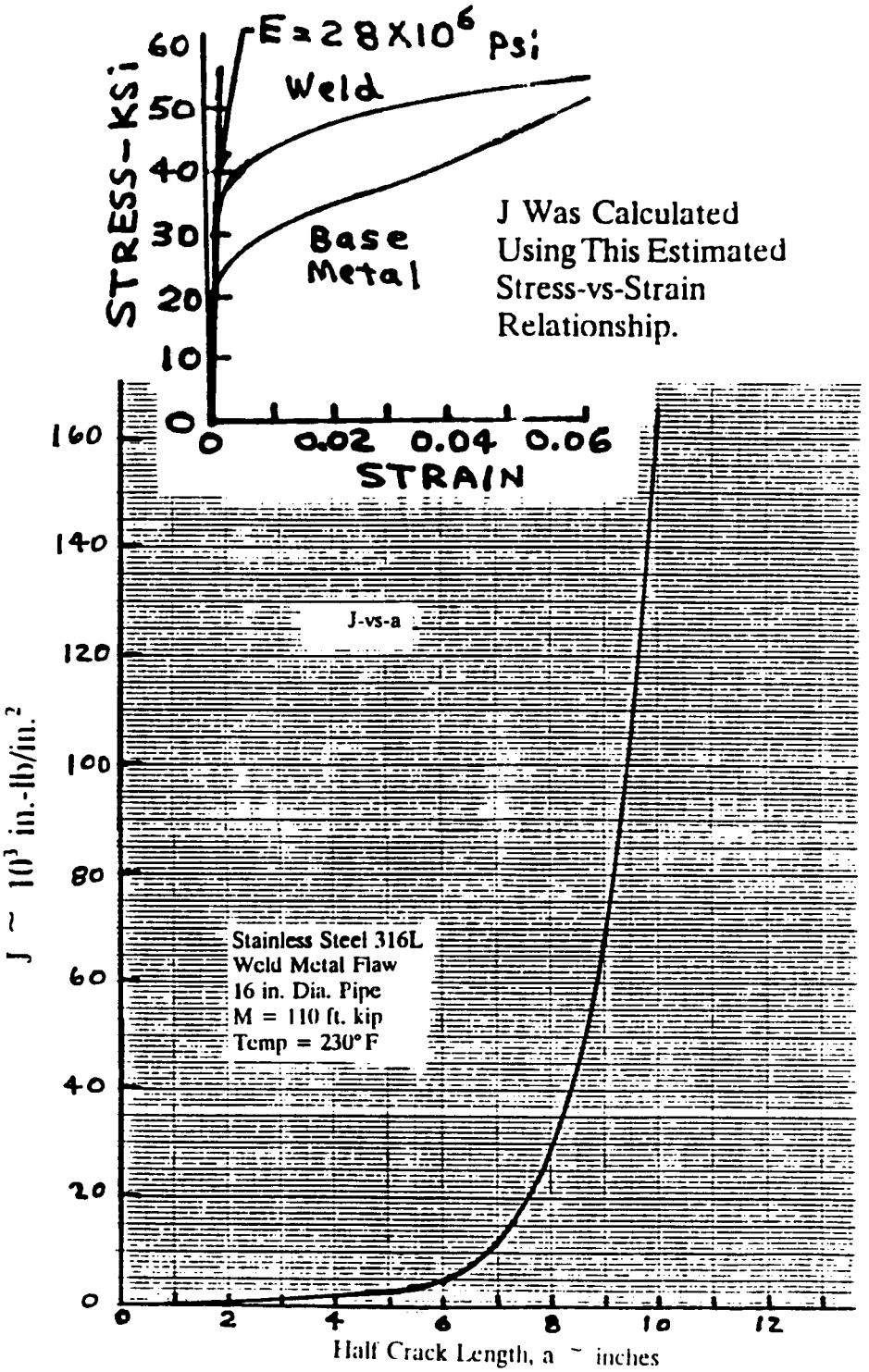

Fig. 30 J Versus Crack Size for Test Pipe

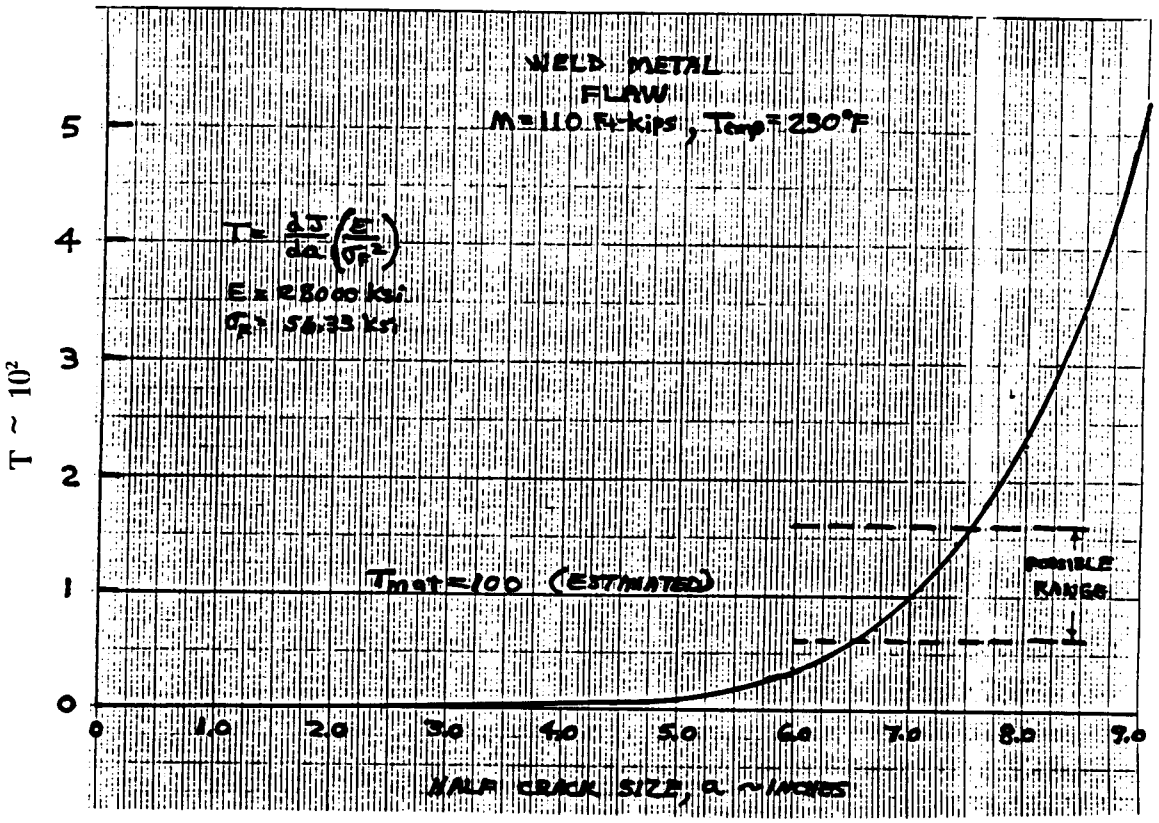

Fig. 31. Tmat Versus Crack Size for Test Pipe

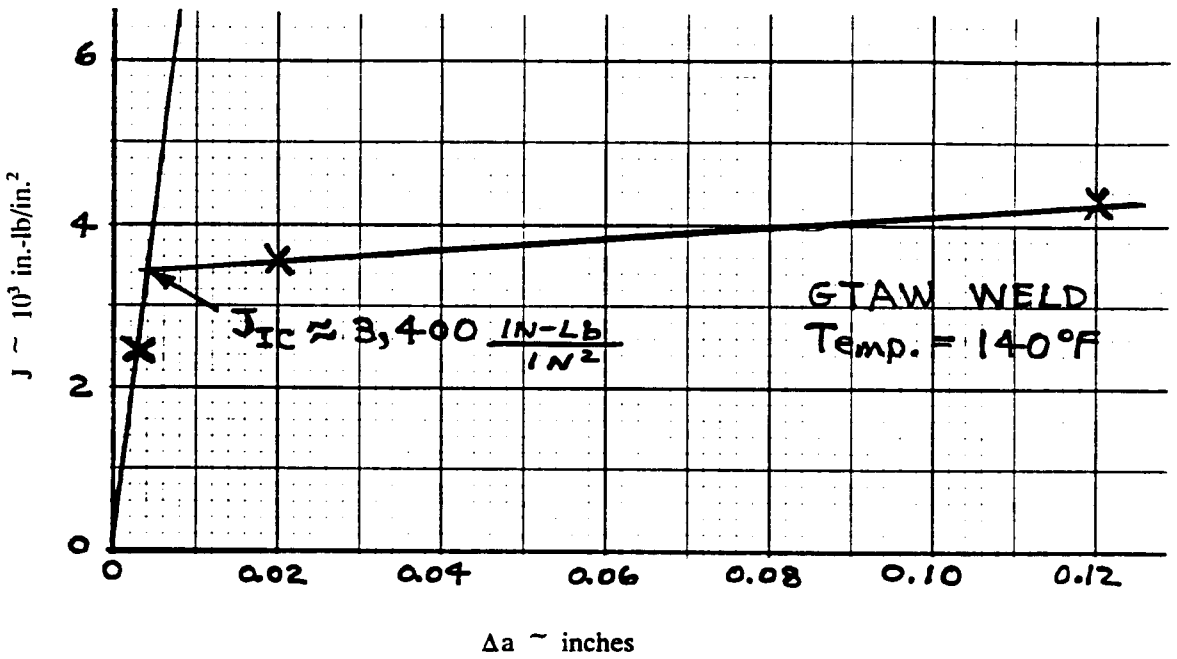

Fig. 32. Estimated J_{IC} for ORNL Compliance Tests

ORNL/NPR-92/8

Internal Distribution

Central Research Library
Document Reference Section
Laboratory Records Department
Laboratory Records, ORNL RC
NPR-RMS-DCC-RC
ORNL Patent Section
G. E. Bell
R. D. Cheverton
J. A. Clinard (5)
J. M. Corum
G. M. Goodwin
R. C. Gwaltney
F. M. Haggag
D. O. Hobson
F. J. Homan
J. E. Jones Jr.
L. M. Jordan
W. J. McAfee
J. G. Merkle
S. E. Moore
D. L. Moses
R. K. Nanstad
D. G. O'Connor
A. B. Poole (5)
T. B. Powell
C. E. Pugh
P. L. Rittenhouse
R. L. Senn
G. M. Slaughter
R. W. Swindeman
W. F. Swinson
D. L. Williams, Jr.
G. T. Yahr
A. Zucker

External Distribution

Argonne National Laboratory, 9700 South Cass Avenue, Building 208, Argonne, IL 60439
L. W. Deitrich
A. E. Klickman

Argonne National Laboratory, Materials Science and Technology Division, Building 212, 9700 South Cass Avenue, Argonne, IL 60493
D. R. Diercks
T. F. Kassner
S. Majumdar
W. J. Shack
R. W. Weeks

Department of Energy/Oak Ridge, Tennessee
L. F. Blankner, Building 4500-N, MS-6269

Department of Energy, Office of New Production Reactors, 1000 Independence Avenue, SW, Washington, DC 20585

K. R. Absher, NP-32
R. J. August, NP-41
J. F. Baker, NP-43
J. M. Broughton, NP-2
J. Hassenfeldt, NP-42
J. J. Jicha, Jr., NP-40 (5)
H. C. Johnson, NP-33
D. E. Kaempf, NP-42
K. A. Klein, NP-30
A. Mehta, NP-44
J. F. Metzler, NP-40
R. J. Neuhold, NP-41
J. R. Rosenthal, NP-42
K. D. Sisson, NP-42
W. A. Stringfield, NP-43
G. Trosman, NP-32

Department of Energy, Barnwell County Project Management Office, Hitchcock Office Park, 35 Varden Drive (NP-70), Aiken, SC 29803

M. C. Kirkland, NP-70

Department of Energy, Hitchcock Office Park, 39 Varden Drive (NP-45), Aiken, SC 29801

J. P. Mulkey

Ebasco Services Incorporated, Two World Trade Center, New York, NY 10048

R. C. Iotti

Lawrence Livermore National Laboratory, P.O. Box 808, Livermore, CA 94551

G. S. Holman

Los Alamos National Laboratory, P.O. Box 1663, Mailstop K-575, Los Alamos, NM 87545

C. R. Bell
W. L. Kirchner
E. Rodriguez

Sandia National Laboratories, P.O. Box 5800, Division 6402, Albuquerque, NM 87185-5800

K. D. Bergeron

Westinghouse - Savannah River Company

K. F. Cooper, 37 Varden Drive, Aiken, SC 29801
J. P. Howell, Savannah River Site, Building 773-41A, Aiken, SC 29802
F. J. McCrosson, Savannah River Site, Building 773-41A, Aiken, SC 29802
C. Thiessen, 37 Varden Drive, Aiken, SC 29801